Pharmacokinetic Modeling of a Liver-Specific Contrast Agent

Alerić, Ivana

SVEUČILISTE JOSIPA JURJA STROSSMAYERA U OSIJEKU

ODJEL ZA FIZIKU

IVANA ALERIĆ

PHARMACOKINETIC MODELING OF A LIVER-SPECIFIC CONTRAST AGENT

Diplomski rad

Osijek, 2018

SVEUČILISTE JOSIPA JURJA STROSSMAYERA U OSIJEKU

ODJEL ZA FIZIKU

IVANA ALERIĆ

PHARMACOKINETIC MODELING OF A LIVER-SPECIFIC CONTRAST AGENT

Diplomski rad

predložen Odjelu za fiziku Sveučilišta J. J. Strossmayera u Osijeku radi stjecanja zvanja profesora fizike i informatike

Osijek, 2018

"This master thesis is made in University hospital Essen under the supervision of PD Dr. rer. nat. Lutz Lüdemann and Assoc. prof.dr.sc. Mladen Kasabašić as part of the Graduate Study of Physics and Computer Science at the Department of Physics of the University of Josip Juraj Strossmayer in Osijek".

Preface

I would like to thank PD Dr.rer.nat. Lutz Lüdemann for giving me opportunity, not only for writing my master thesis under his mentorship, but also gain new knowledge and experience. As well as to Dr. Lüdemann I would like to thank to my second mentor doc.dr.sc. Mladen Kasabašić. Specially I would like to thank Dipl.Phys. Stefan Hindel for introducing me with fresh and effective methods of work in science. Besides them, I want to thank to Dominik Geisel and Tim Denecke for providing access to data and images. I would also like to thank M. Sc. Patrick Zylka for introducing me with the subject and help when it was necessary.

At the end I would like to thank to my family and friends from Croatia who was encouraging me during my entire stay in Essen, as well as my friends from Essen who were real support in this part of my life.

Sveučilište J. J. Strossmayera u Osijeku
Odjel za fiziku

Diplomski rad

FARMAKOKINETIČKO MODELIRANJE SPECIFIČNOG KONTRASTA ZA JETRU

IVANA ALERIĆ

Sažetak:

Mjerenje funkcije jetre nakon embolizacije temelji se na primjeni specifičnog kontrasta za jetru, koji se putem jetre izlučuje u žuč te snimanjem cijelog procesa magnetskom rezonancom. Zatvaranjem jednog kraka portalne vene koja omogućuje dovod hranjivih sastojaka, potiče se rast drugog dijela jetre koji na sebe preuzima funkciju djela zaraženog tumorom. Analiza snimaka magnetske rezonance, koja se sastoji od nekoliko faza, daje krivulje koje predstavljaju vremensku promjenu koncentracije kontrasta u krvi i tkivu jetre. Primjenom farmakokinetičkih modela za opisivanje krivulja dobivamo parametre koji opisuju funkciju jetre; perfuziju, brzinu apsorpcije te izlučivanja kontrasta, volumen hepatocita te sinusoidalnih stanica.

Rad je pohranjen u knjižnici Odjela za fiziku
Ključne riječi: "embolizacija", "farmakokinetički modeli", "jetra", "magnetna rezonanca"
Mentor: PD Dr. rer. nat. Lutz Lüdemann, Doc.dr.sc. Mladen Kasabasic
Ocjenjivači:
Rad prihvaćen:

J. J. Strossmayer University in Osijek
Department of Physics

Master of Physics Thesis

PHARMACOKINETIC MODELING OF A LIVER-SPECIFIC CONTRAST AGENT

IVANA ALERIĆ

Abstract:

Measurement of liver function after embolization is based on the application of specific liver contrast agent which can be excreted through liver into the bile and recording the whole process with magnetic resonance. By closing the branch of the portal vein which enables food supply, we stimulate the growth of the second, healthy, part of the liver. The analysis of MRI recordings consists of several phases and gives curves that represent time-varying contrast concentrations in blood and liver tissue. By using pharmacokinetic models for fitting the curves we obtain parameters that describe the function of the liver; perfusion, contrast uptake and extraction rate, volume of hepatocytes and sinusoidal cells.

Thesis deposited in Department of Physics library
Keywords: "embolization", "pharmacokinetic models", "liver", "magnetic resonance imaging"
Supervisor: PD Dr. rer. nat. Lutz Lüdemann, Doc.dr.sc. Mladen Kasabasic
Reviewers:
Thesis accepted:

Contents

List of Tables

List of Figures

1 Introduction

Portal vein embolization is medical procedure used before hepatic resection. Before hepatectomy, functional liver remaining has to reach the sufficient size necessary for liver regeneration after surgery. Preoperative embolization of the portal vein which feed the hepatic segments reduced the risk of postoperative liver failure after liver resection. The aim of embolization is complete obstruction of the targeted branches and redistribution of flow to the future liver remain. Radiologist places a needle into the liver and when he identify blood vessels, inject small microspheres into the vessel to block blood supply. The size of the particles is 300μm to 900μm. The procedure is frequently used in primary liver cancer or colorectal liver metastases (Romaric Loffroy 2015).

Global assessment of liver function is assessed by laboratory tests such as ICG (indocyanine green) test or LiMAx (maximum liver function capacity) test. Postoperative liver residue is examined by volume using CT or MRI because tests are limited when liver function is not homogeneously distributed. One of techniques for image-based liver function estimation is dynamic contrast-enhanced MRI. Distribution of contrast agent can be easily displayed by magnetic resonance imaging (MRI) with high temporal and spatial resolution (D. Geisel 2015).

In this master thesis it will be explained principle of magnetic resonance and origin of the MR images. I will describe blood supply in the liver because it is crucial for understanding of contrast agent flow. In section about methods are

shown data processing steps of the recordings. The aim of the work is investigate pharmacokinetic models which can best describe uptake, pathway and excretion of liver specific contrast agent, so in contiuation are shown fitting procedure, models and the results processed by individual models.

2 Theoretical background

2.1 Basic principles

The most abundant atom in human body is hydrogen because it is one of the component of water and fat. Hydrogen consist of electron which orbit a positive nucleus. Electron and nucleus are also spinning around their own axis. Since the nucleus contains positively charged proton, due to nuclei spin, nuclei can be consider as a small magnet because of electromagnetic induction. Magnetic moment of each nuclei can be described with vector which represents the direction and size of magnetic moment. When these magnetic active nuclei are not in the presence of magnetic field their orientations are random, but when we apply some external magnetic field B_0 they tend to align with the field. Depending on their energy, magnetic moment of the nuclei will align parallel or anti-parallel (Figure 2.1).

The influence of external magnetic field causes the precession of the magnetic moments around B_0. Precessional frequency ω_0 or so called Larmor frequency depends on external magnetic field B_0 and gyromagnetic ratio γ:

$$\omega_0 = B_0 * \gamma \cdot \tag{2.1}$$

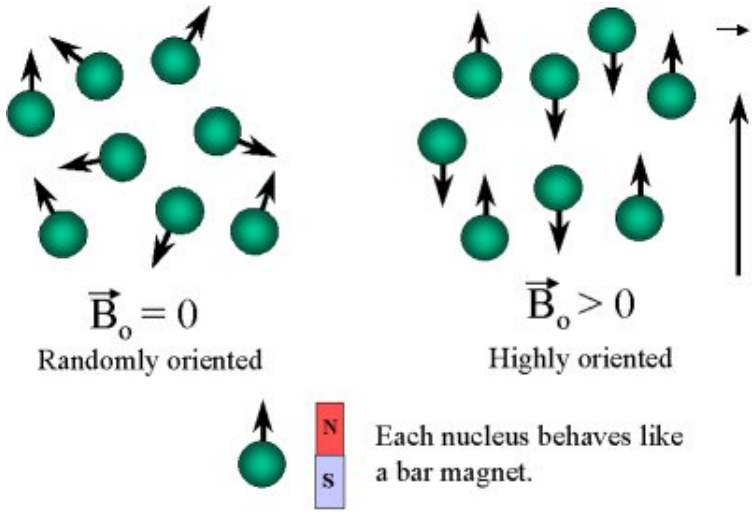

Figure 2.1: Orientation of nuclei magnetic moments. Nuclei with higher energies will align anti-parallel, while nuclei with lower energy states will align parallel to B_0. (The University of Meine)

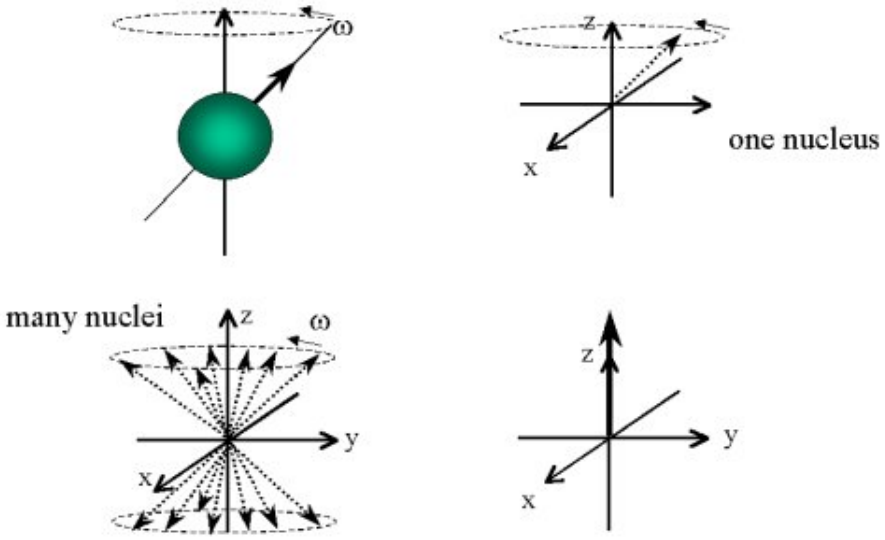

Figure 2.2: Precession of magnetic moments with frequency ω (The University of Meine)

.

The nucleus can gain energy only if it is equal to energy of precession of the spin. Energy of hydrogen corresponds to the radio frequency from $10^6 Hz$ to $10^9 Hz$, so the application of a radio frequency (RF) pulse will cause excitation. Excitation results in more nuclei in a higher energy state. Resonance also causes magnetic momentum vectors to no longer lie parallel to B_0. The angle

to which vector shifts out of alignment is called flip angle and depends on the RF pulse. The other result of resonance is coherence; the vectors are moving in phase and generate the MR signal when cutting across the coil. That process induces electric signal. Therefore, signal intensity is proportional to the amount of magnetization present in transverse plane.

After RF pulse, magnetic vectors lose coherency and recover their longitudinal magnetization. T1 recovery is caused by nuclei giving up their energies to the surrounding lattice. It is exponential process in which *T1 relaxation time* represent the time it takes 63% of the longitudinal magnetization to recover in the tissue. T2 decay represents the loss of coherent transverse magnetization which can also be described with exponential function. *T2 relaxation time* is point when the 63% of transverse magnetization is lost (Catherine Westbrook 2011).

2.2 Pulse sequence

Dephasing is not caused only by nuclei losing energy, but also with inhomogeneities in tissue. Inhomogeneities are areas which do not match the external magnetic field and that affects the Lamour frequency. Inhomogeneity produce rapid loss of coherent transverse magnetization and signal. To measure relaxation the signal has to be recovered and there are two ways for doing this - using a 180° RF pulse or using gradients.

The spin echo pulse sequence uses 90° excitation pulse to flip the magnetic vector in the transverse plane. Right after the 90° RF pulse, T1 recovery and dephasing starts. To compensate dephasing, a 180° RF pulse is applied. The 180° RF flips individual magnetic moments for 180 degrees so that the leading ('fastest')

vector becomes the trailing ('slowest') vector while the direction of precession remains the same. This transverse magnetization induces signal in the coil and it is called *spin echo*.

The gradient echo pulse sequence uses an RF excitation pulse and flips the magnetic vectors through any angle, mostly less then 90°. That means that the transverse component of magnetization is smaller then in spin echo because only one part of longitudinal vectors are completely flipped to transverse plane. After the RF pulse, relaxing signals are produced. The magnetic moments in transverse plane starts dephasing, but instead of 180° RF pulse, vectors are rephased by gradient. The gradient causes changes in magnetic field strength and produces coherence. This signal is called a *gradient echo* (Catherine Westbrook 2011).

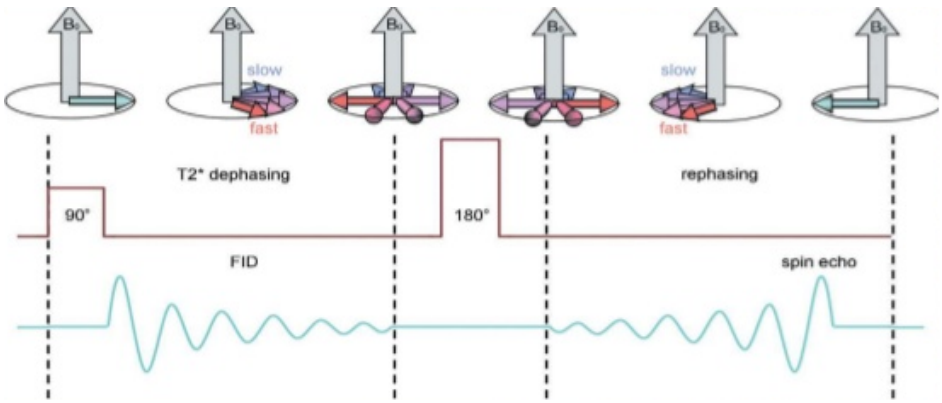

Figure 2.3: A basic rephasing sequence (Catherine Westbrook 2011)

2.2.1 Gradient echo pulse sequence

Magnetic field gradients are generated by coils situated within the bore of the magnet. Through every coil passes electric charge and induces magnetic field which interacts with the main magnetic field. Whether a gradient field increases or decreases, main magnetic field depends on the direction of current passing through gradient coils. Gradient can be activated in 3 directions; x,y and z axes.

The magnetic isocentre is the point of 3 axes where precession frequency remains unchanged. In the main magnetic filed all nuclei has the same Larmor frequency, because they experience the same magnetic field. When they experience gradient magnetic filed their precession frequency is changed and they lose a coherence. If gradient is applied to incoherent vectors it can increase the precession frequency of the 'slower' vectors, and decrease the precession frequency of 'faster' ones. Gradient magnetic field can be subtracted from B_0 or added to B_0 and form steep or shallow slopes. Gradient can be used for more purposes; besides dephasing and rephasing in pulse sequence they preform slice selection, frequency encoding and phase encoding.

Gradient echo enables faster imagining. T*2 decay is caused by static dephasing effects, which occur because of susceptibility of tissues (T'2 decay), and time variant field fluctuations between magnetic moments of neighboring spins (T2 decay). Spin echo imagining can nullified T'2 dephasing effects because 180° RF pulse which corrects static field imperfections. Those imperfections can not be refocused with gradient echo so that T*2 includes T2 and T'2 effects and the signal will decay much faster (Michale Markl 2012). TR is time between two excitation pulse and together with flip angle controls T1 relaxation. TE is time between excitation and signal and it effects on T2* decay. If we want to get *T1 weighting image* we have to maximize the difference in T1 times of the tissues. To obtain *T2 weighting image* we have to maximize T2* differences i.e. TE should be long enough so vectors can decay and show the differences. Flip angles and TR should be short. To get *proton density weighting* T1 and T2* processes are minimized so that we use short TE and long TR because we do not want recovery of magnetization. (Catherine Westbrook 2011)

2.2.2 FLASH imagining

Magnetic resonance measuring with long measuring times result with motion artifacts and they can not give us information about fast physiological processes. There are few rapid techniques of imagining, but they have low signal to noise ration (SNR) or require large number of RF pulses. Fast low angle shot (FLASH) imaging has optimal SNR, reduced measuring time and good spatial resolution. Main difference between other MRI techniques and FLASH is the use of RF pulses with low flip angles which eliminate waiting periods between excitation. Instead of excitation entire longitudinal magnetization FLASH technique excite only small part of it. With every pulse available longitudinal magnetization is separated into transverse part and remaining longitudinal part. TR and TE can be as much short as hardware of gradient system allows it. TE is time between RF pulse and highest peak of signal. Imaging time depends on number of desired projection, duration of slice selection and acquisition of data (A.Haase 1986).

During FLASH imaging RF pulses are applied together with gradient which affect only certain slices of object in one direction (G-slice). Spatial discrimination in second direction comes from presence from perpendicular gradient which cause the free induction decay (FID) (G-read) and creates gradient echo signal. Phase-encoding gradient (G-phase) preforms spatial encoding in the second dimension what we can see on Figure 2.4. (David Stark 1999).

2.2.3 Keyhole filling

K space is spatial frequency domain in which we can store the frequency signals from MRI. It has 2 axes; phase axis is vertical and the frequency axis is hori-

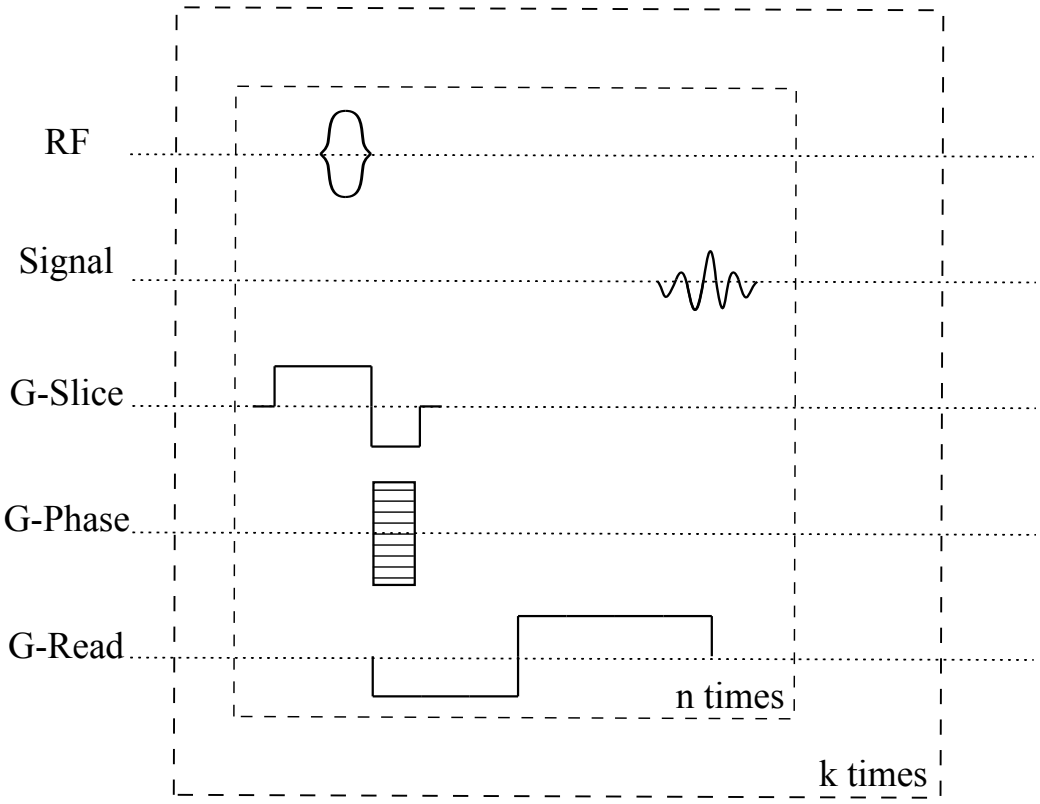

Figure 2.4: FLASH imaging

zontal (Figure 2.5. For every phase one line in K space is filled. Fast Fourier transformation enables obtaining of MRI images from data in K space. The sampled data correspond to $N_x \times N_y$ matrix, where N_x represents the number of frequency data points and the N_y represent the number or TR times.

The reduced k-space filling, also known as keyhole imaging, represents technique for shortening the acquisition time of the MR data. This technique minimizes the number of TR steps by replacing the missing data points in K-space. The low spatial frequencies with high amplitudes and low phase shifts in the central region determine the coarse structure. The high spatial frequencies in the outer region give us the detailed information. (Zahif 2014)

With TWIST technique it is possible to achieve improvements in temporal and spatial resolution in shorter time relative to other dynamic imaging. To shorten

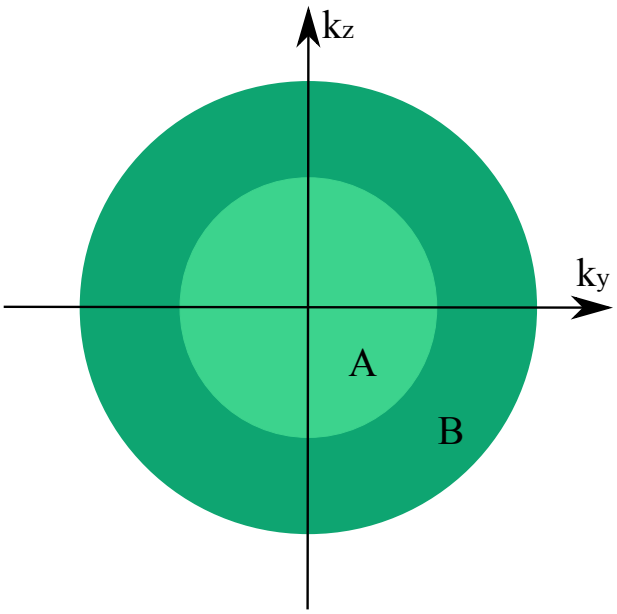

Figure 2.5: K space

time TWIST sequence use short TR, reduce spatial resolution, partial Fourier, apply rectangular field of view and use parallel imaging. To increase the temporal resolution we can manipulate with the amount of data during acquisition. It is not necessary to cover the whole K space during converting signals. K space can be divided into two sections; A region which includes low frequency and carry the information about contrast and B region which includes high frequency responsible for image details. Since temporal resolution depends on total number of K space multiplied by TR, to improve it, we have to reduced the number of data from region B. (Gerhard Laub 2006)

2.3 Liver physiology

Liver is the largest organ in human body. It is divided into right and left lobe by falciform ligament and contains eight sections. On the inferior liver surface next to gall bladder is attached quadrate lobe and the caudate lobe is placed to

the posterior surface. Liver is very perfused organ with high blood flow which is needed for delivering oxygen. Three main vessels are placed in the liver; hepatic artery, hepatic portal vein and central vein (A.C.Guyton 2006). Liver is supplied with blood from two different sources. Hepatic artery carries around 30% of the blood while the portal vein, which is much thicker then artery, gives around 70% of blood. This division is described as an arterial flow fraction (J.Sear 1992).

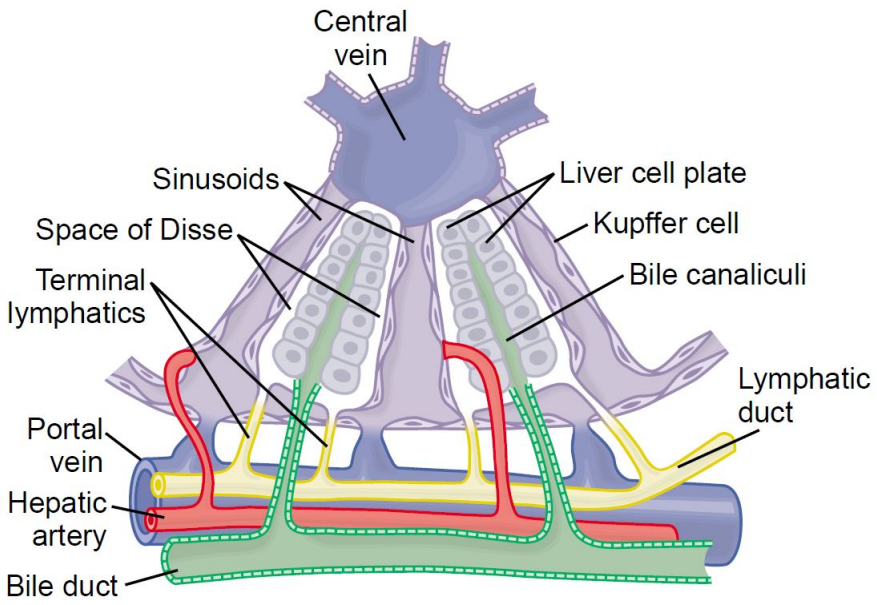

Figure 2.6: Structure of liver lobule with cellular plates, blood vessels, bile collecting system and lymph flow system. (A.C.Guyton 2006)

Hepatic artery comes from heart and carries oxygen into the liver. Portal vein, supplies liver with nutrients from gastrointestinal tract, but also toxins and partly deoxygenated blood. Liver releases nutrients back into the blood through sinusoids and central vein. Liver contains 3 main components; sinusoids, hepatocytes and bile canaliculus. Blood from hepatic artery and portal vein enters the sinusoids. Sinusoidal cells are open porous blood space. Around them are tightly packed hepatocytes which enables easy access to the blood. The hepatic sinusoids mix and send blood to a central vein from where it flows through a hepatic vein into the inferior vena cava. Blood flow and bile flow are in oppo-

site directions. Sinusoidal cells also contains Kupffer cells which remove dead blood cells, bacteria and other toxic material that enter the sinusoids. Between sinusoidal cells and hepatocytes is separation called space of Disse. Hepatocytes build liver and they take up around 80% of total liver volume (OpenStax College 2013). These cells have more that one role in the liver. They are involved in protein anabolism and catabolism in zone in which they receive high oxygenated blood, but if they are placed in zone with poor oxygenated blood, they will preform biotransformation of drugs. The products of the hepatocytes, like bile and bilirubin, will be drained into the bile canaliculus and to the bile duct, while proteins and lipids will be extracted to sinusoids or stored up in cells (J.Sear 1992).

2.4 Gadolinium contrast agents

Every voxel has signal whose strength is represented with grey scale, lighter voxels represent stronger signals. The contrast in MR images is showing differences between tissues. If pictures are T1 weighted the water will be shown dark and the fat light. On T2 weighted pictures both fat and water are shown light. Depending on the tissue which we want to examine we have to use certain way of imagining. To have stronger contrast between the tissues it is possible to use contrast agent which is changing T1 and T2 relaxivity of the tissue. First developed liver specific contrast agents had role to improve contrast to noise ratio between metastases and healthy liver tissue. Since lesions have less functional hepatocytes which can not exert uptake of contrast media, signal in these areas will be decreased. Depending on the way of accumulation and concentration in the tissue we can make conclusions about perfusion and diffusion in body. There are positive contrast agents which have increasing signals and negative contrast

agents with decreasing signals. Most of contrast agents are positive and based on Gd^{3+} which is paramagnetic metal. Gadolinium has seven unpaired electrons which also have spin and magnetic moment which is 657 times stronger then the one of proton. The interaction between gadolinium and hydrogen atoms allows fast releasing of protons energy and thus better relaxation. Because of recovery of longitudinal magnetization signal in T1 images is increasing (Zylka 2013).

Ionic gadolinium has toxic effect on muscles and blood so that we could use it, it has to be in molecular state which would prevent uptake of gadolinium. The binding does not take place via a chemical bond, but by an inclusion of the gadolinium ion in a molecular envelope. The chemical composition of Primovist, Gadolinium based contrast agent also called gadoxetate disodium, is shown in figure below. Liver specific contrast agents are used for detection and morphological characterization of lesions but also for anatomy and function of the liver.

There is a difference between intravascular and extravascluar contrast agents whose kinetics are determinated only by perfusion and diffusion, and also metabolizable contrast agents which are taken up by the Kupffer cells. This contrast agent has two kinetic phases; distribution and elimination. It can be administrated as intravascular bolus and it enables the imagining of vascular structures and focal lesions. While contrast agent is distributing in the compartments it is possible to preform imagining of hepatic artery and portal vein phase. Gadocetic acid is actively transported from sinusoidal cells via organic anion transporting polypeptide into the hepatocytes. After that they are excreted in biliary canaliculi. Because of these characteristic it provides anatomic and functional information about liver diseases (Yee Liang Thiana 2013). The plasma half life of Gd-EOB-DTPA is approximately 56 minutes in patients with healthy liver. Experiments which are preformed on rat's livers shown that T1 relaxivity of

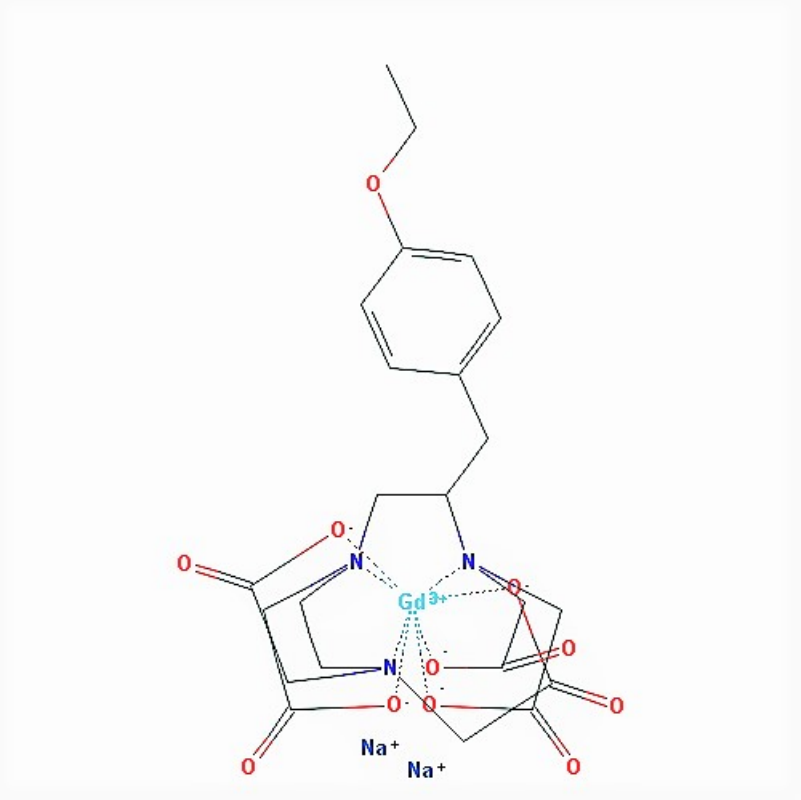

Figure 2.7: 2D structure of Primovist (Pubchem)

.

Gd-EOB-DTPA in liver is 16.6 L/mmol and in blood 11.2 L/mmol (Bernard E. Van Beers 2012).

3 Methods

3.1 Motion correction

During the acquisition time, due to patient's breathing, organs are changing their position and shape. For data processing, it is necessary to average the voxels signals from different liver voxels and that process requires one position of the liver. With software ProSoma is preformed an elastic motion correction of the static and dynamic images. In automatic coregistration, coregistration is performed based on normalized mutual information. For reference image we selected T1-weighted high-resolution VIBE sequence. The aim is to couple the high resolution of the VIBE sequence with the functional information of the dynamic sequence.

Voxel-based motion correction compares the gray value information of the two data sets. Used metric is based on entropy, which is a measure of the uncertainty of the occurrence of a particular event from a group of events. Event represents the occurrence of a gray value, while the probability that this event occurs is the relative frequency of the gray value. The overlap of the entropies of both sets of images provides the information. This is called a common entropy. Thus, for each combination of gray values occurring in the overlapping area of both images, it is necessary to determine the relative frequency with respect to all gray value combinations. It is possible to overlap the images with a very

small entropy or decreasing entropy of the secondary data set. The common information of both images, that is, the overlap, is maximized to minimize the common entropy. This ensures a more stable coregistration, but is not yet free from misregistration which occurs when the individual entropies change more than the common entropy. The avoidance of these errors is achieved with using the normalized mutual information (NMI), which is determined by the following equation:

$$NMI_{Ref,Sek} = \frac{H_{Ref} + H_{Sek}}{H_{Ref,Sek}} \tag{3.1}$$

where H_{Ref} is the entropy of the primary reference data and H_{Ref} is entropy of the secondary transformed data. (Butzek 2014)

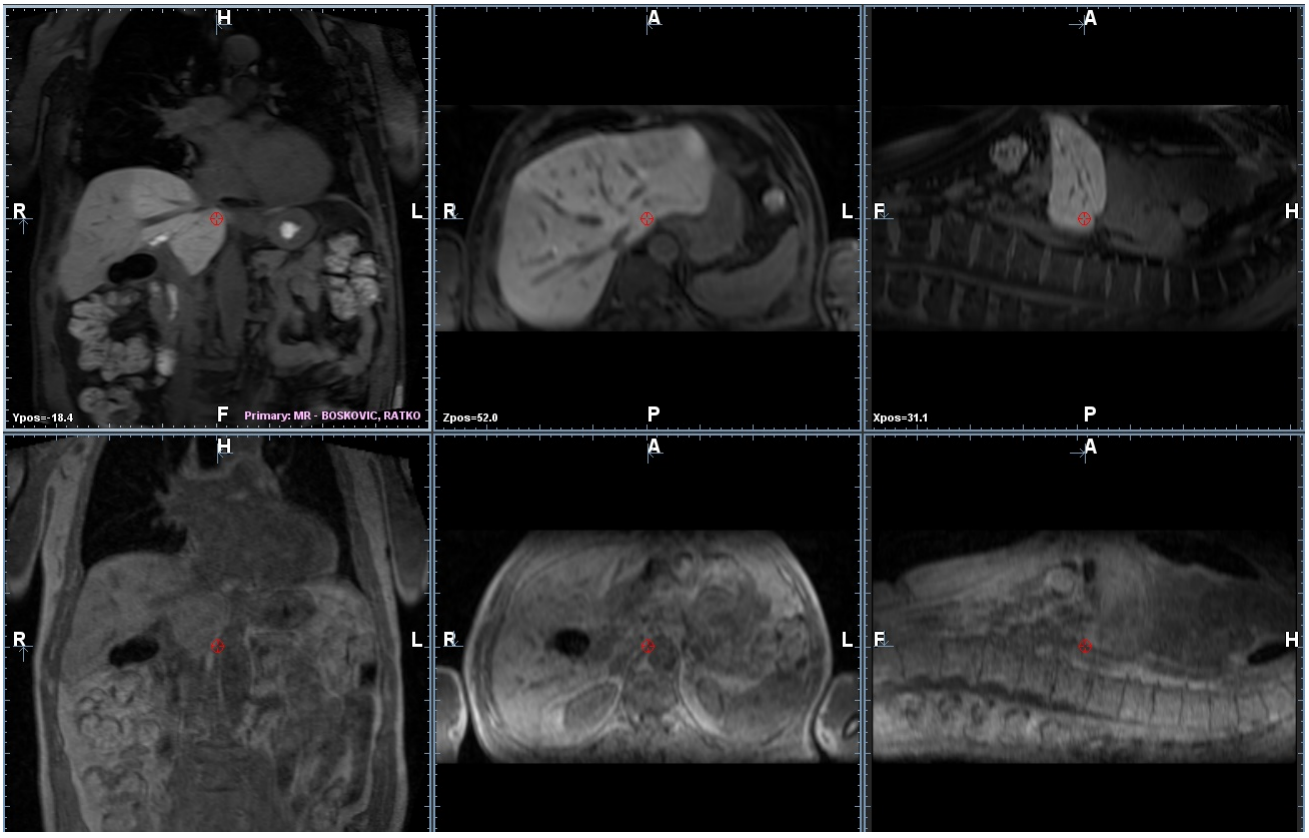

Figure 3.1: Motion correction in ProSoma; Primary data (first row) and secondary data (second row).

There is a possibility for choosing between Fast and High Quality motion correction. If case of High Quality, a second calculation step is carried out after coregistration by means of NMI, which coregistrates the images on the basis of their intensity values. This leads to errors in multimodal image data, so only the Fast option was used. (Butzek 2014)

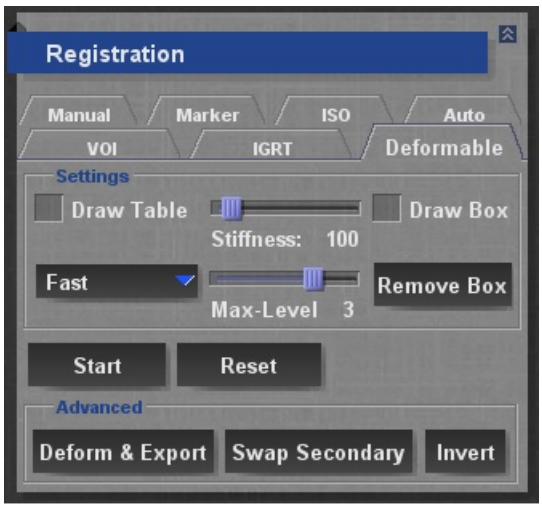

Figure 3.2: Settings for motion correction in ProSoma.

3.2 Creating $\triangle$R1 maps

Contrast agent signal intensity in tissue depends on the concentration of the agent. Signal intensity depend on the pulse sequence, acquisition duration and homogeneity. Signal increases with CA concentration and it is shown in ΔR1 map. Signal changes from T1 weight images enable calculating concentrations and producing contrast time curves. Maps of proton density M_0 and longitudinal relaxation rate $R1_0$ maps were calculated using 5 sets of GRE images with different flip angles

$$s(\alpha) = M_0 sin\alpha \frac{1 - E1_0}{1 - cos\alpha E1_0} \tag{3.2}$$

where α = 5°, 10°, 20°, 30°, 35°.

R1(t) maps represent four-dimensional longitudinal relaxation rate is calculated from dynamic data sets prom pre-contrast and post-contrast T1 weighted images using equation

$$R1(t) = -\frac{1}{TR} ln \frac{1-(A+B)}{1-cos\alpha(A+B)}, \tag{3.3}$$

where α=35°,

$$A = S(t) - \frac{S(0)}{M_0 sin\alpha} \tag{3.4}$$

and

$$B = \frac{1-E1_0}{1-cos\alpha E1_0} \tag{3.5}$$

while S(t) and S(0) are signal intensity of 4D T1 weighted images (Ka-Loh Li 2000).

3.3 Selection of region of interest (ROI) and extraction of signal time curves

Next step in analysis of MR images is defining specific areas of liver and blood vessels. Since it is possible to distinguish tissues by signal strength, setting the threshold show 'active' regions. ROIs are defined by structural or functional features. Structural ROIs are based on anatomy and the best way to get them is to define them for each subject. Functional ROIs are based on analyzing individuals. Common approach is to use scan to identify and compare voxels and their response in different manipulations (Poldrack 2007).

There is several different methods for extraction of ROIs. When selecting areas it is important not to include border zone voxels which can have influence in partial volume effect. Because of high flow in the middle of the vessels signal is

also higher so for the best balance it is also necessary to include voxels closer to vessel walls. Selection can be preformed manually from different types of images and semi-automatic based on anatomy maps and tractography (Ylva Lilja 2016).

While selecting ROIs I combined anatomy characteristics with setting threshold of signal intensity on typical values for certain tissue and then manually selected ROI. Relaxivity value R1 in blood at magnetic field strength of 1.5 T for Primovist is 7.3 L/mmol*s (Martin Rohrer 2005). During passage of first and second bolus relaxivity values are considerably higher and because of this I relied on anatomical features. From ΔR1 maps I extracted time steps in which intensity of certain area was the highest. On extracted file I marked one test area with full blood volume for material statistic in which I could saw minimum and maximum intensity of signal. These values were used for setting threshold and masking specific areas which I included in ROI. Once when threshold is setted it is easy to mark ROI through slices (Figure 3.4.

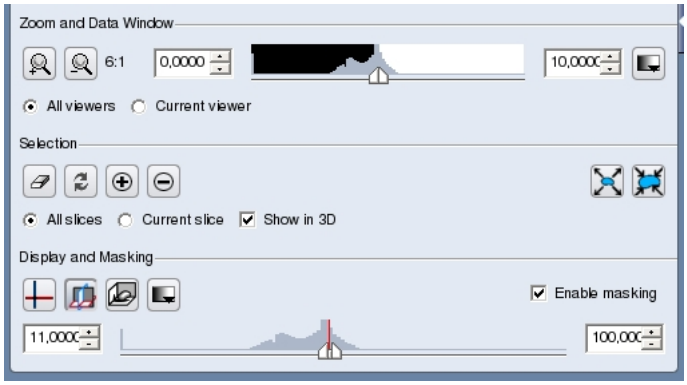

Figure 3.3: Display and Masking settings in software Amira52. Threshold is setted from minimum to approximately maximum values from test area.

From every ROI one signal time curve S(t) can be calculated, with time signal drop during the CA passage, by averaging all voxels signals in the region. Signal time curves can later be converted into the concentration time curves C(t) which

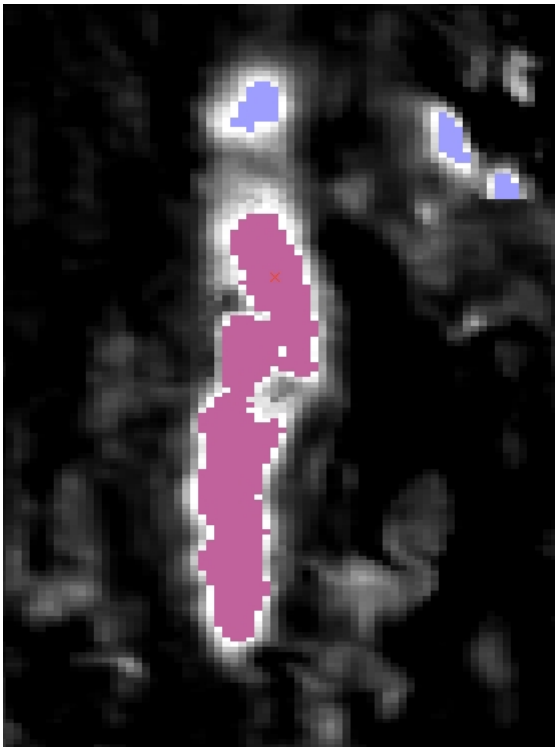

Figure 3.4: Purple areas represent masked signals. These areas are only possible for marking but it is necessary choose only ones which surely represent certain tissue.

represent concentration of CA in the blood. Equation used for converting signal time curves which came from ΔR1(t) maps into concentration curves is

$$C(t) = \frac{R1(t) - R1_0}{\Re 1}, \tag{3.6}$$

where R1(t) is

$$R1(t) = \frac{1}{T1(t)}. \tag{3.7}$$

$\Re 1$ is relaxivity of Gd-DTPA-BMA and $R1_0$ baseline relaxation signal intensity. T1 is value of longitudinal relaxation rate (Ka-Loh Li 2000). Relaxivities used in calculations are taken from literature (Bernard E. Van Beers 2012).

3.4 Gamma variate function

Gamma variate function is function which is used for describing passage of contrast media bolus through vessels and tissue. It is used for fitting process of the signal time curves of arterial input function and portal vein input function. The gamma variate function is expressed as:

$$\gamma(t) = \begin{cases} A(t-t_0)^{\alpha} e^{(-\frac{t-t_o}{\beta})}, & t > t_0 \\ 0, & t \leq t_0 \end{cases} \tag{3.8}$$

where t represent time and t_0 delay time from $t = 0$ to the beginning of the slope on the curve. In our case t_0 is the time between injection of CA and appearance of the bolus in the liver. In fitting process, A, α and β are setted as free parameters. A is magnitude of the curve. α and β affect on the slope of the fit in first bolus pass, but also on location and amplitude of the maximum (Madsen 1992).

Signal time curves consist of first bolus pass, second bolus pass and saturation. Second bolus and saturation are consequence of the recirculation of the CA in the human body after the first bolus. Usually, second bolus arrive 15 to 20 seconds after first bolus. (Thomas Benner 1997). Concentration in blood plasma is sum of first component $C_{p,b}(t)$ and second $C_{p,mix}(t)$ component when contrast agent is well mixed in blood. Concentration of CA in blood during first pass bolus is usually fitted with Gamma-variate function.

$$C_{p,b}(t) = \begin{cases} C_{b,0}(t-t_0)^{\alpha} e^{(-\frac{t-t_o}{\beta})}, & t > t_0 \\ 0, & t \leq t_0 \end{cases} \tag{3.9}$$

Like in Gamma variate function, $C_{b,0}$ represent magnitude of the curve. α and β determine the slope first bolus pass. The second component of single time curve

can be shown as single exponential increase and biexponential decrease.

$$C_{p,mix}(t) = \begin{cases} \sum_{i=s,f} C_{mix,i0}(1 - e^{-\psi(t-t_o-\Delta t)})e^{-\chi_i(t-t_o-\Delta t)}, & t > t_0 + \Delta t \\ 0, & t \leq t_0 + \Delta t \end{cases} \tag{3.10}$$

α, β, ψ and χ are fitting parameters which describe the time course. Δt is time shift between first and second bolus (L. Lüdemann 2000).

Code in Appendix A represent loop for fitting arterial signal time curves. Gamma variate function was used for first and second bolus. Modified equation for second bolus was used for saturation. For fitting portal vein signal time curves is also used Gamma variate function but only for one bolus and saturation. Main part of the code is in Appendix A. Curves and their fits are shown on Figure 3.5.

3.5 Pharmacokinetic modeling in MRI

Clinically applied semi-quantitative pharmacokinetic models which result in physically unclear transport parameters for tracers used in dynamic contrast enhanced MRI were developed in 1990s (Tofts u. a. 1999). Models of the newer generation use parameters as perfusion and capillary permeability.

An indicator is substance which yields physiological informations about the system and tracer is type of indicator which is chemically identical to system but detectable from system. MR contrast agents (CA) are indicators but not a tracers. Assuming that some tissue has inlets and outlets carrying the substances, transit time is time between entrance of the particle in and exit out of the tissue. Probability distribution of transit times is represented by $H(t)$ and the

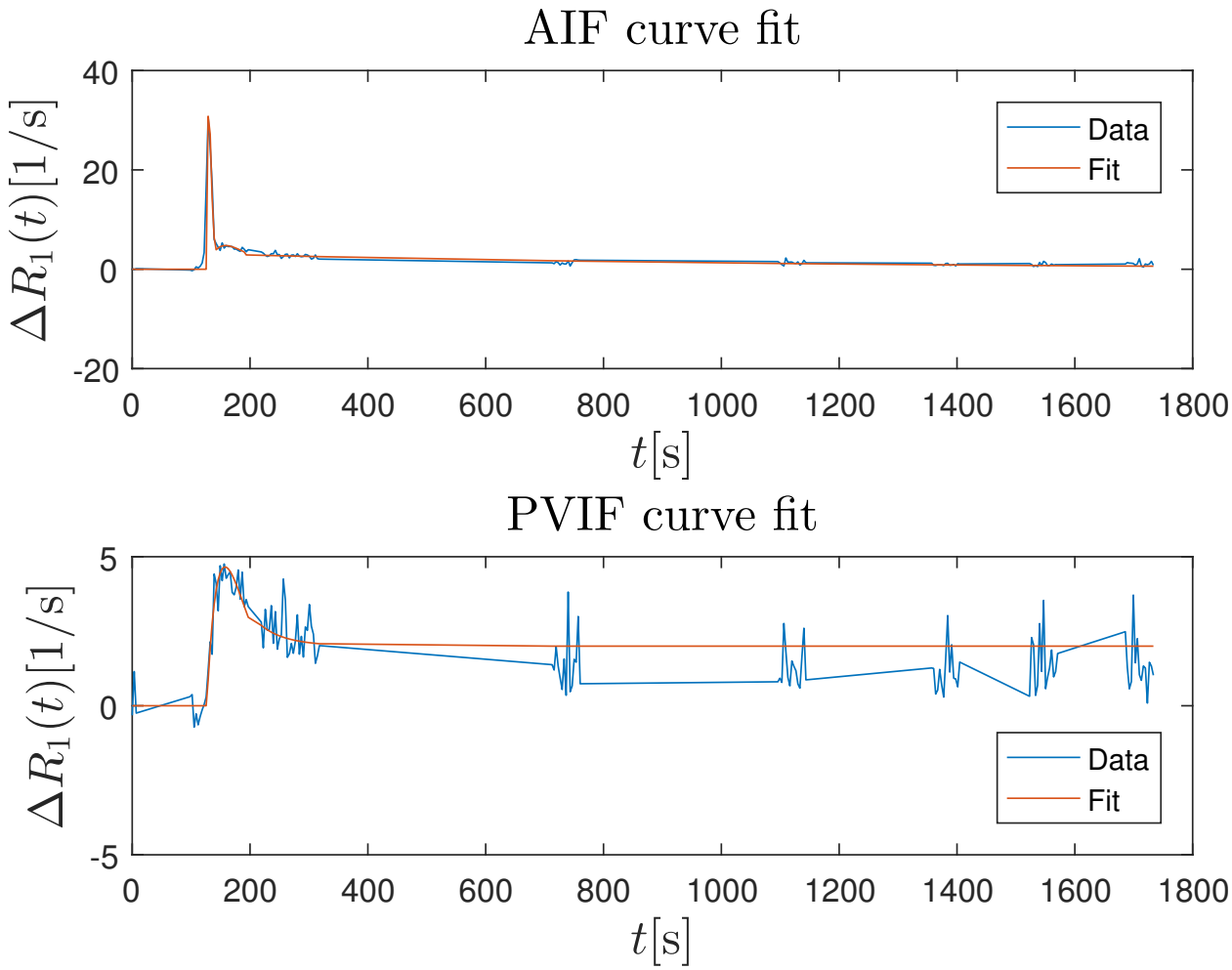

Figure 3.5: Results of fitting AIF and PVIF signal time curves (Patient 9)

mean transit time (MTT) is the expectation value of $H(t)$. Tissue concentration C is the amount of contrast agent in the sample divided by the volume of the sample. It is possible to use normalized volume of distribution v and define a concentration $c(t)$ as amount of contrast agent in the sample divided by volume of distribution v what is showed in relation

$$C(t) = vc(t). \tag{3.11}$$

The flux of contrast agent which is transported through the tissue is described like amount of contrast agent per unit of time. Change of amount of total CA in the blood is difference between total influx $\sum J_i(t)$ and total outflux $\sum J_o(t)$. If

we apply law of conservation on the flux definition we will get

$$\frac{dC(t)}{dt} = \sum_{i \in inlet} J_i(t) - \sum_{o \in outlets} J_o(t)\cdot \tag{3.12}$$

Definition of compartment is well-mixed space where the concentration is spatially uniform within the volume of distribution. In compartment model the influx of contrast agent can be defined as flow F multiplied with concentration $c(t)$. By combining this with equation for conversation of the flux we get

$$v\frac{dc(t)}{dt} = \sum_{i \in inlet} F_i c_i(t) - \sum_{o \in outlets} F_o c_o(t)\cdot \tag{3.13}$$

Capillary models, except venous outlet, assume leakage of CA through capillary walls what is actually second outlet of CA into the extravascular extracellular space (EES). The permeability P represents outflux of CA per unit wall area and per unit concentration and it is approximately same along the capillary wall. In that case outflux through capillary wall $J_l(t)$ is the product of permeability-surface area and average concentration of CA. (S.P.Sourbron 2011a)

3.5.1 One compartment model

One of the capillary models is compartment model which assume that capillary bed is compartment. c_p represent the concentration of CA in v_p so the leakage flux which goes from capillary wall to EES is product of surface permeability PS and concentration $c_p(t)$

$$J_l = PSc_p(t). \tag{3.14}$$

If we assume that flux of CA in plasma volume is equal to sum of the influx, outflux and permeability outflux we will get balance equation for compartment model:

$$v_p\frac{dc_p(t)}{dt} = F_p c_p(t) - F_p c_p(t) - PSc_p(t). \tag{3.15}$$

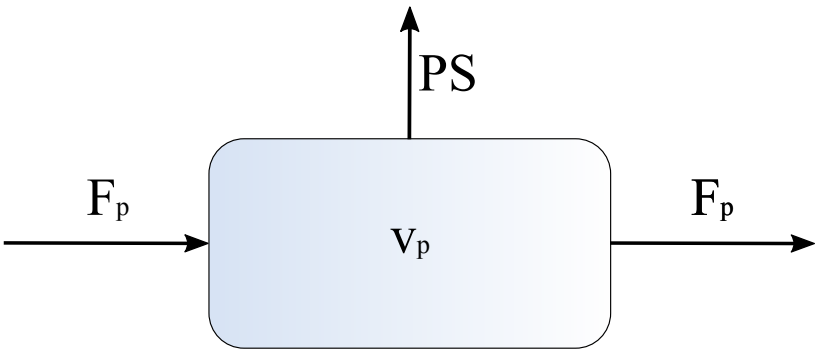

Figure 3.6: Compartment model

3.5.2 Tissue uptake model (TU)

The tissue uptake model is special case of two-compartment exchange model, but we assume that in this case there is no exflux of CA from EES back to plasma. Since the outflux of CA to EES is inconsiderable small, mean transit time T_e is longer then time of measurement so that parameters T_e and v_e can not be measured precisely. Also, concentration of CA in plasma volume is much larger than that in the EES volume because only inlet to EES is through capillary wall. Mass balance equation for TU model is expressed like:

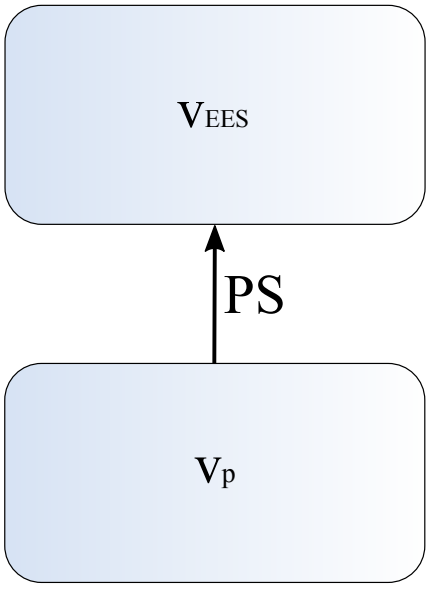

Figure 3.7: Tissue uptake model

$$v_e \frac{dc_e(t)}{dt} = PSc_p(t) \tag{3.16}$$

where c_e represent concentration in interstitial volume v_e (Jesper F. Kallehauge 2017).

3.5.3 Dual-inlet two-compartment uptake model

Two region models assume that CA is passing from one compartment into another; it will be extracted from vessels through the capillary wall to EES and cells.

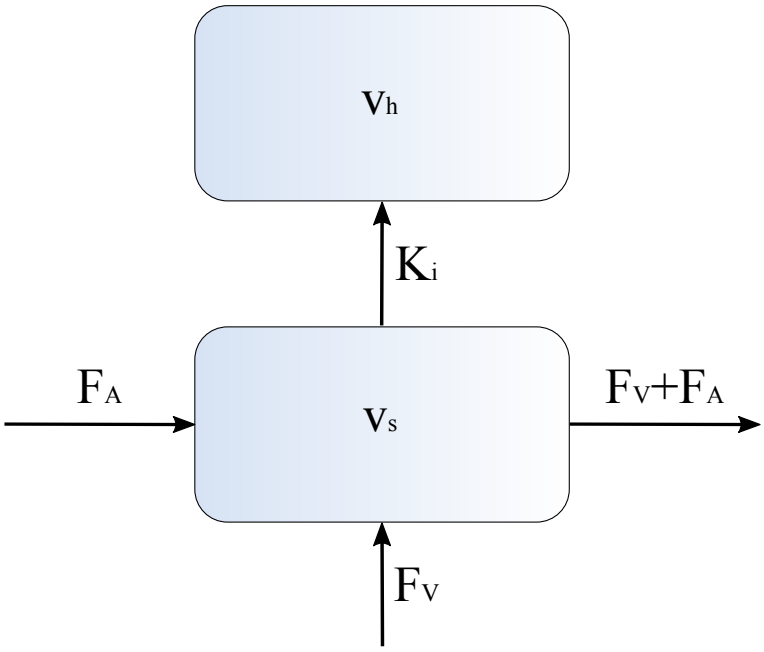

Figure 3.8: Dual-inlet two-compartment uptake model

Since is well known that gadoxetic acid is taken up by hepatocytes from plasma i.e. sinusoidal cells instead of plasma volume and volume of extracellular extravascular space, it will be used sinusoidal volume and hepatocytes volume. Contrast agent have 2 inlets; arterial and venous (S.P. Sourbron 2012). Main contribution comes from venous plasma flow f_v, but signal in liver is increased before bolus in portal vein. To sum up arterial and venous flows we have to implement new parameter f_a; arterial flow fraction:

$$c_s(t) = f_a c_a(t) + (1 - f_a)c_v(t). \tag{3.17}$$

This expression turns two-inlet model into single-inlet model. Model assume that arterial input function (AIF) is sampled directly in capillary bed but in practice arrival is delayed. It is obvious in case of poor fit and it can be corrected with artery and venous delay;

$$c(t) = c(t - T_0). \tag{3.18}$$

Surface permeability is included in model as uptake rate K_i of contrast agent from sinusoids to hepatocytes (S.P.Sourbron 2011a). Concentration of contrast

agent in v_s and v_h can be described by combining equations for compartment model and tissue uptake model.

$$v_s \frac{dc_s(t)}{dt} = F_{a+v} c_{a+v}(t) - F_{a+v} c_s(t) - K_i c_s(t) \tag{3.19}$$

$$v_h \frac{dc_h(t)}{dt} = K_i c_s(t) \tag{3.20}$$

Main part of fitting routine is placed in Appendix A.

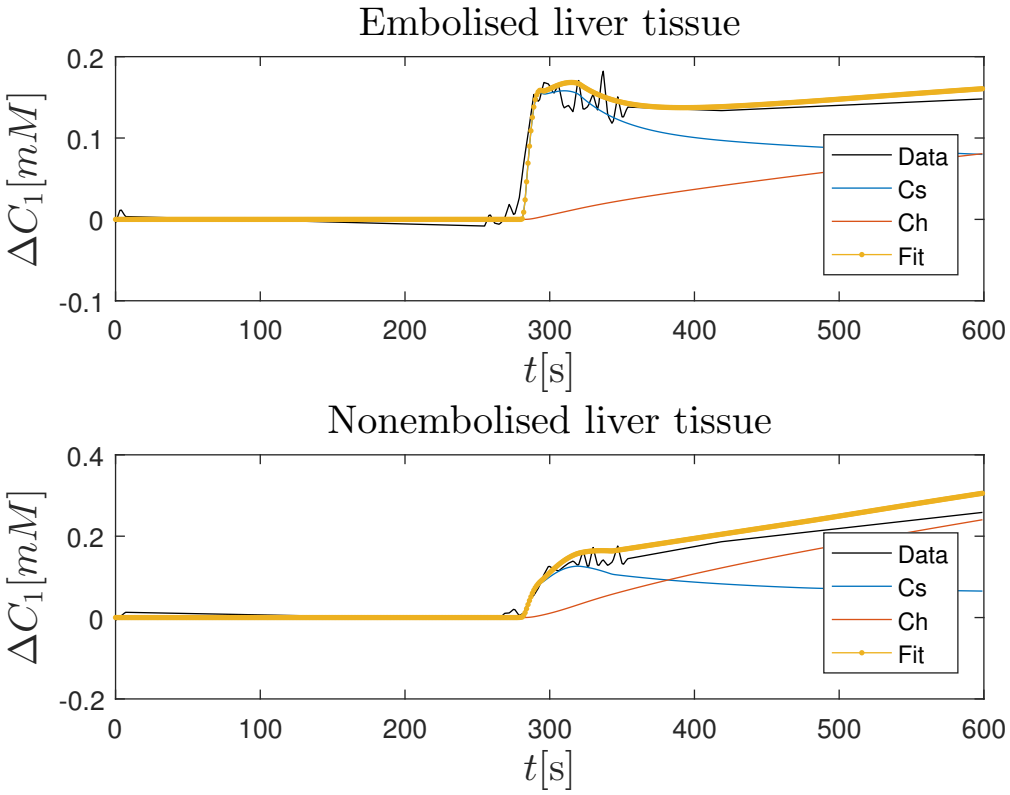

Figure 3.9: Results of fitting liver tissue signal time curves with dual-inlet two-compartment uptake model [600 s]; since this model describe only uptake of CA acquisition duration is setted to only five minutes; (Patient 9)

3.5.4 Dual-inlet two-compartment uptake model with extraction rate K_e

Gadoxetic acid has to be extracted from hepatic cells into the biliary pathway. Parameter K_e is describing the excretion of contrast agent. Extraction rate is much smaller than uptake rate because of filtration of blood from toxic and unnecessary components.

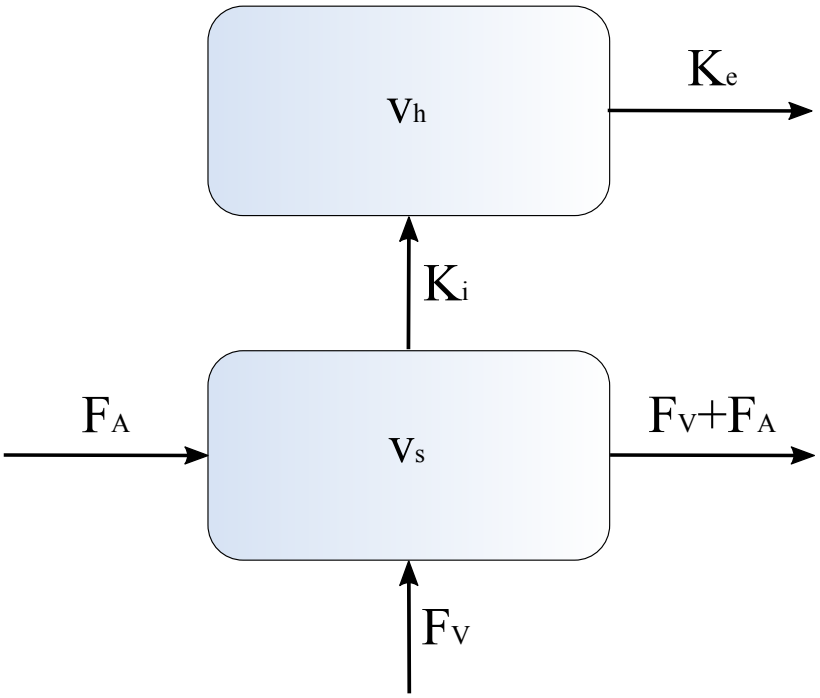

Figure 3.10: Dual-inlet two-compartment uptake model with extraction rate K_e

The arterial flow fraction and extraction rate can be included in equations used for dual-inlet two-compartment model. We get set of equations which are consist of 6 fitting parameters; sum of arterial and venous flow (F_{a+v}), sinusoidal volume (v_s), uptake rate (K_i), hepatocytes volume (v_h), arterial flow fraction (f_a) and extraction rate (K_e).

$$v_s \frac{dc_s(t)}{dt} = F_{a+v}(f_a c_a(t) + (1 - f_a)c_v(t))(t) - F_{a+v}c_s(t) - K_i c_s(t) \quad (3.21)$$

$$v_h \frac{dc_h(t)}{dt} = K_i c_s(t) - K_e c_h(t) \tag{3.22}$$

Because of complexity of the model I excluded delay from fitting parameters and set it as constant; $Delay_a = 1$ and $Delay_p = 1$. It is necessary to include delay of one second into the fitting process to get more correct values of other fitting parameters. Values $c_a(t)$ and $c_v(t)$ are taken from fitted AIF and PVIF signal time curves at every single time point t.

The total concentration C is the combination of concentration of CA in the sinusoidal volume, c_s and the hepatocytes volume, c_h:

$$C(t) = v_s c_s(t) + v_h c_h(t). \tag{3.23}$$

In Appendix A it is placed main part of fitting routine and Figure 3.11 shows data curve and fitting curves. This model describe uptake and extraction of CA and acquisition duration is around 15 minutes.

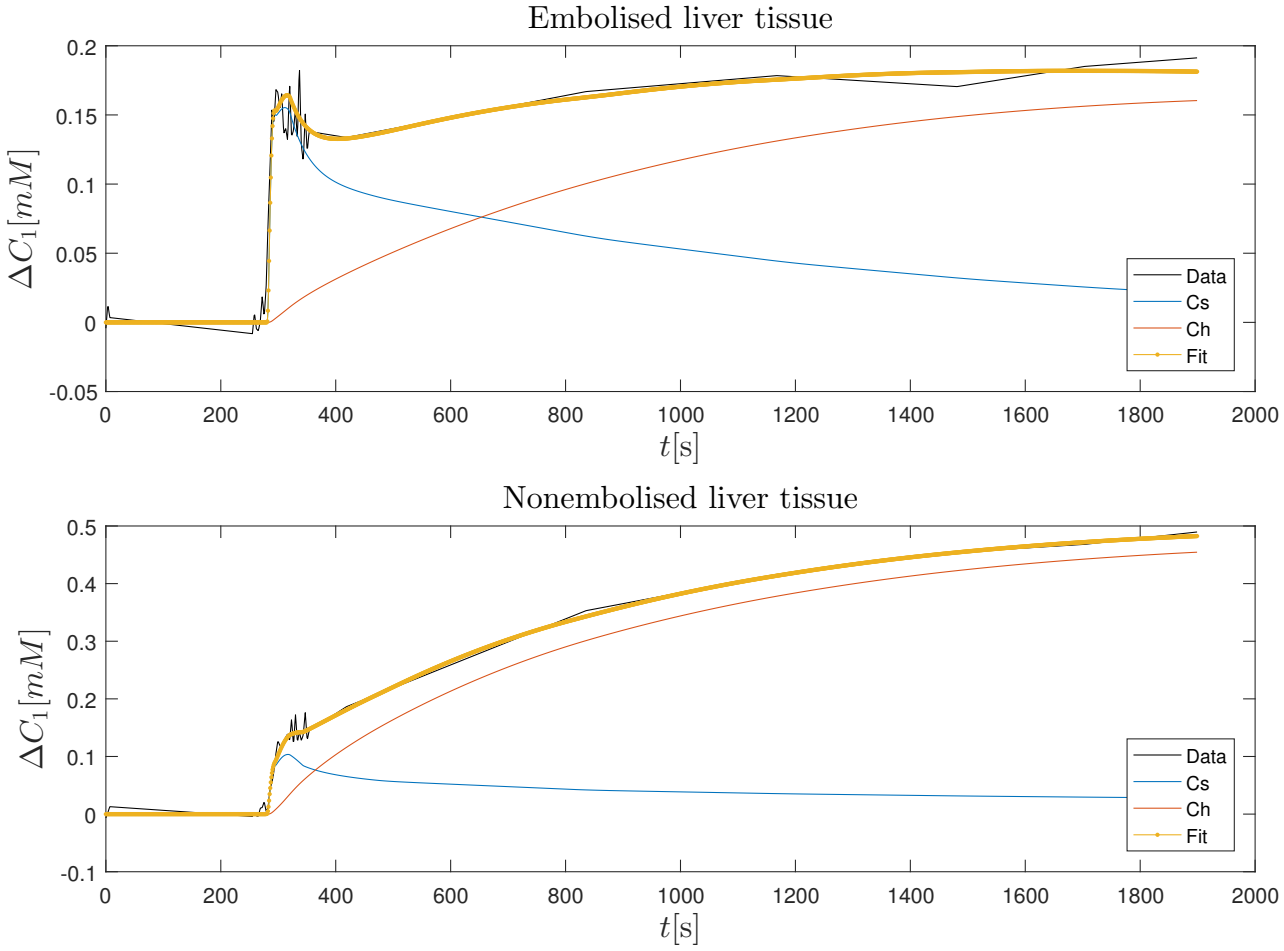

Figure 3.11: Results of fitting liver tissue signal time curves with dual-inlet two-compartment uptake model with extraction rate (Patient 9)

4 Material

4.1 Patients

A study was conducted to examine patients with various malignant disease in liver that required portal vein embolization. This method is useful in cases when surgical tumor removal is not possible due to the size or location of the tumor without maintaining sufficient residual function of the liver. In this type of intervention individual branches of the portal vein are mechanically closed in order to prevent the high blood supply in the malignant area. As a result highly blood-perfused, healthy portion attempts to compensate for the diminished overall function and grows steadily. Once sufficient size and function of the healthy liver lobes are present, the malignant areas can be surgically removed without unduly compromising liver function as a result of the surgery.

Patients have been advised of possible risks and have submitted a statement of consent for the use of their data for research purposes. Several anatomical and dynamic sequences were performed, both with and without contrast medium. The total examination time should not exceed 45 minutes as far as possible. For my research I used data of 12 patients where 6 of them are female and 6 male. All of them had primary tumor of the liver or metastases on the liver.

Table 4.1: Informations about patients age, sex and acquisition duration

Patient	Age	Sex	Aquisition duration[s]
Patient 1	59	Female	1900
Patient 2	55	Female	1600
Patient 3	66	Male	1900
Patient 4	69	Male	1700
Patient 5	59	Male	1600
Patient 6	71	Male	1550
Patient 7	48	Male	1500
Patient 8	65	Female	1800
Patient 9	56	Female	1900
Patient 10	59	Female	1600
Patient 11	70	Female	1700
Patient 12	68	Male	1700

4.2 MR sequence

All images were taken in a MR tomograph from Siemens at 1.5T magnetic field strength. As a transmitting and receiving coil was used a combination of a Siemens 6-channel body coil and the table coil of the MR scanner. For each patient's study, 19 different MR sequences were used for both anatomical and dynamic imaging. For evaluation, seven gradient echo sequences were used, which are subsequently broken down after the time of recording. The first five sequences were run before the contrast agent administration. These are the TWIST[21] sequences required for the excitation angle method with excitation angles of 5°, 10°, 20°, 30° and 35°.

The sixth sequence is the dynamic sequence. It is divided into three shots before contrast administration and 135 shots taken during and after contrast administration. The time interval between two images is on average 3.4 seconds. Longer recording pauses in the dynamic sequence were used to drive anatomical se-

Table 4.2: Sequence parameters of all sequences used for data evaluation

Sequence number	1-5	6	7
Sequence type	TWIST static	TWIST dynamic	VIBE static
Flip angle	5°, 10°, 20°, 30°, 35°	30°	10°
T_R	2,33ms	2,33ms	2,33ms
T_E	0,84ms	0,84ms	0,84ms
Acquisition matrix	205 x 256	205 x 256	338 x 512
Image resolution	256 x 72 x 256	256 x 72 x 256	512 x 60 x 512
K-Space rows	24	24	24

quences. The duration from the recording of the first to the last dynamic image data set was about 20 minutes. The number and order of shots has been preset, the duration of the breaks varies depending on the patient and the personnel performing the task.

The seventh sequence is an anatomical T1-weighted VIBE[22] sequence. It was made 20 minutes after contrast administration. This recording is taken with breath hold and serves as a reference recording for movement correction of the liver.

4.3 Methods evaluation

For evaluation of methods I compared mean root squares (RMS) of fitted curves with F-test. It is hypothesis test used for comparing two models from witch one

of them is simpler and other more complex. In equation

$$F = \frac{(SS_s - SS_c)/SS_c}{(DF_s - DF_c)/DF_c} \tag{4.1}$$

$DF = N - K$ represent degree of freedom where N is the number of data points and K is the number of free parameters. If the simpler model is correct F-test result is around 1. If the ratio is much greater than 1, more complicated model is correct or the simpler model is correct, but more complicated model to fit better. If the P value is low, more complex model is statistically significantly better (P. Kletting 2009).

5 Results and discussion

For examination of liver function of 12 patients I used two methods; dual-inlet two-compartment uptake model (2CUM) and dual-inlet two-compartment uptake model with extraction rate (2CUMEX). All patients were successfully imaged and analyzed. These models had some variations in acquisition duration and boundaries for fitting volume parameters. Since volume of hepatocytes and sinusoidal cells are known from the literature ($v_h = 74\%$, $v_s = 16\%$) these could be setted as fixed value instead of fitting parameters (Renz 2003). In addition to get better fit I also setted volumes as parameters with low boundaries (5% from literature values) and high boundaries (30% from literature values). 2CTUM was used in 2 different acquisition duration; 600 s and 1700 s (mean value of acquisition duration for every patients), while 2CTUMEX had to use all time points because of extraction which demands more time then just and uptake.

Values of RMS in embolised and nonembolised tissue and degrees of freedom for every model are shown in Table 5.1.

Table 5.1: Root mean square values and degrees of freedom

	2CUM[600s]		
	Fixed v_h, v_s	Fitted v_h,v_s(LB)	Fitted v_h, v_s (HB)
Degree of freedom	60	58	58
RMS$_{emb}$	0.00009669	0.00007690	0.00004481
RMS$_{nemb}$	0.00012659	0.00012002	0.00005706

	2CUM[AD]		
	Fixed v_h, v_s	Fitted v_h,v_s(LB)	Fitted v_h, v_s (HB)
Degree of freedom	65	63	63
RMS$_{emb}$	0.00018343	0.00005870	0.00002292
RMS$_{nemb}$	0.00015962	0.00015115	0.00005292

	2CUMEX[AD]		
	Fixed v_h, v_s	Fitted v_h,v_s(LB)	Fitted v_h, v_s (HB)
Degree of freedom	64	62	62
RMS$_{emb}$	0.00007674	0.00004369	0.00003064
RMS$_{nemb}$	0.00004644	0.00004487	0.00002919

It is necessary to have different degree of freedom for comparison of models with F-test, and model with low fitting boundaries obviously have larger RMS values, so I reject all results with low fitting boundaries and compare ones I got with fixed values and high boundaries fitted values. Results are shown in Table 5.2.

Table 5.2: F-test values; upper results refers to embolised tissue and below on nonembolised tissue

F-Test			
Simpler method	Complex method	F-test result	p value
2CUM [600] Fixed	2CUM [600] Fitted	33.57	<0.00001
		35.33	<0.00001
2CUM [AD] Fixed	2CUM [AD] Fitted	220.61	<0.00001
		63.51	<0.00001
2CUMEX [AD] Fixed	2CUMEX [AD] Fitted	46.65	<0.00001
		18.32	<0.00001

Results of F-test indicate that values we got with fitted parameters are better because of low p-values. Next step was compare which one of models in case of fitting volumes is the best. Results are show in Table 5.3.

F-test values point to the fact that 2CUM in acquisition duration of 600 seconds better describes liver function. The reason is smaller number of fitting parameters and smaller degree of freedom. Since 2CUM does not describe contrast agent extraction but only absorption, the excessive degree of freedom during 1700 seconds measurement caused a bad result in F-test with comparison to 2CUMEX. Still, 2CUMEX model gives pretty good fit, value of one more parameter and better describes longer acquisition time liver curves.

Table 5.3: F-test values; upper results refers to embolised tissue and below on nonembolised tissue

F-Test			
Simpler method	Complex method	F-test result	p value
2CUM [600] Fitted	2CUM [AD] Fitted	-12.04	-
		-0.98	-
2CUM [600] Fitted	2CUMEX [AD]	-7.17	-
	Fitted	-14.80	-
2CUM [AD] Fitted	2CUMEX [AD]	-15.61	-
	Fitted	50.40	<0.00001

5.1 2CUM[600 s]

Mean value and SD from 2CUM in acquisition duration of 600 s of perfusion (total plasma flow per blood volume) is 65.5±32.1 for nonembolised tissue and 26.2±15.7 for embolised tissue what we can see in Table 5.4. There is significant difference between perfusion in liver tissues (P=0.001) what means that nonembolised tissue is highly perfusion compared to embolised. Extracelular volume in nonembolised and embolised tissue is 29.5±6.3 and 22±6.9. Hepatocytes volume contains 63.1±4.6 in nonembolised and 65.3±4.4 in embolised. Sinusoidal volume differences between tissues are significant (P=0.01) but there is no difference when it comes to hepatocytes volume. It is to be expected that the sinusoidal volume, which represent the blood volume, will be greater in nonembolised tissue because it is more perfused. Uptake rate is significantly bigger in nonembolised tissue (P<0.00001); 7.9±3.4 and 1.9±1.2 for embolised. Values are in range with literature values (S.P. Sourbron 2012). Arterial flow fraction in embolised tissue is always 100 while in nonembolised tissue 22±19.4. Figure 5.1 shows results in boxplots.

Table 5.4: Statistical results for 2CUM[600s]

	F[ml/min/100ml]		v_s[%]		v_h[%]	
	NEmb	Emb	NEmb	Emb	NEmb	Emb
Median	62.8	20.6	31	20.7	61.9	65.3
Mean	65.5	26.2	29.5	22	63.1	65.3
Standard deviation	32.1	15.7	6.3	6.9	4.6	4.4

	K_i[ml/min/100ml]		f_a[%]	
	NEmb	Emb	NEmb	Emb
Median	7.6	2.2	18	100
Mean	7.9	1.9	22	100
Standard deviation	3.4	1.2	19.4	0

5.2 2CUM[AD]

The dual-inlet two compartment model gives values for perfusion 38.2±19.4 and 26.3±15.6 for nonembolised and embolised tissue (Table 5.5). There is no significant difference between tissues flow (P=0.11) what telling us one more time that this fit does not describe data good enough because it is not possible to distinguish liver parts. T-test of root mean square between tissues confirms this fact (P=0.006). Fits are not good for one of the tissue, in this case for nonembolised. Values for volume and arterial fraction in nonembolised part of the liver are hitting lower and upper boundaries, probably because this model can not describe saturation perfectly. Volume of sinusoidal cells and uptake rate is again larger in nonembolised tissue (P<0.0001) and hepatocyte volume is smaller in nonembolised part (P=0.02).

With dual-inlet two compartment model in duration of approximate 1700s is possible to check dependence of parameters on time acquisition. Literature indicates that with increase of acquisition duration parameter values will increase

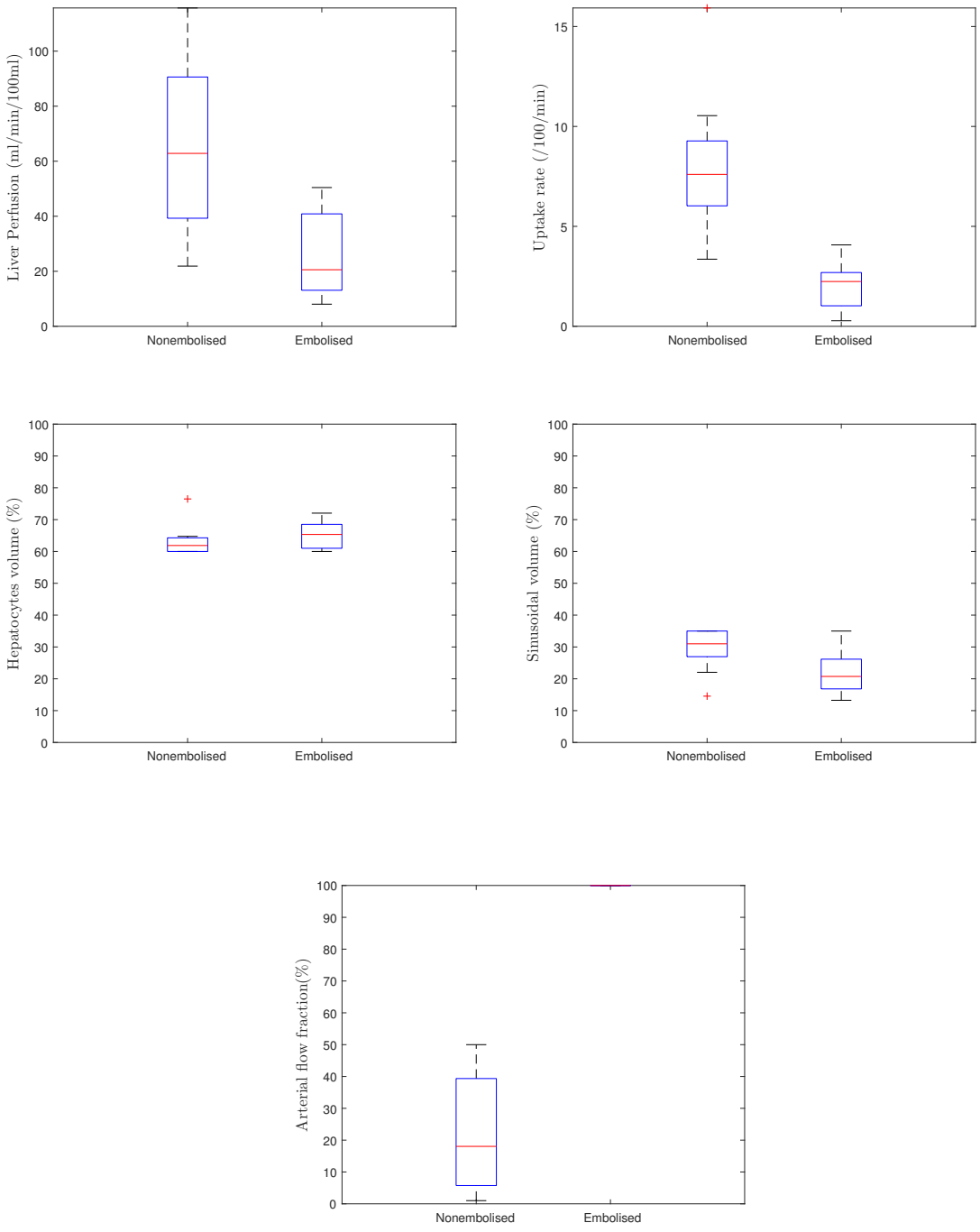

Figure 5.1: Parameters values given with dual-inlet two compartment model in acquisition duration of 600 s

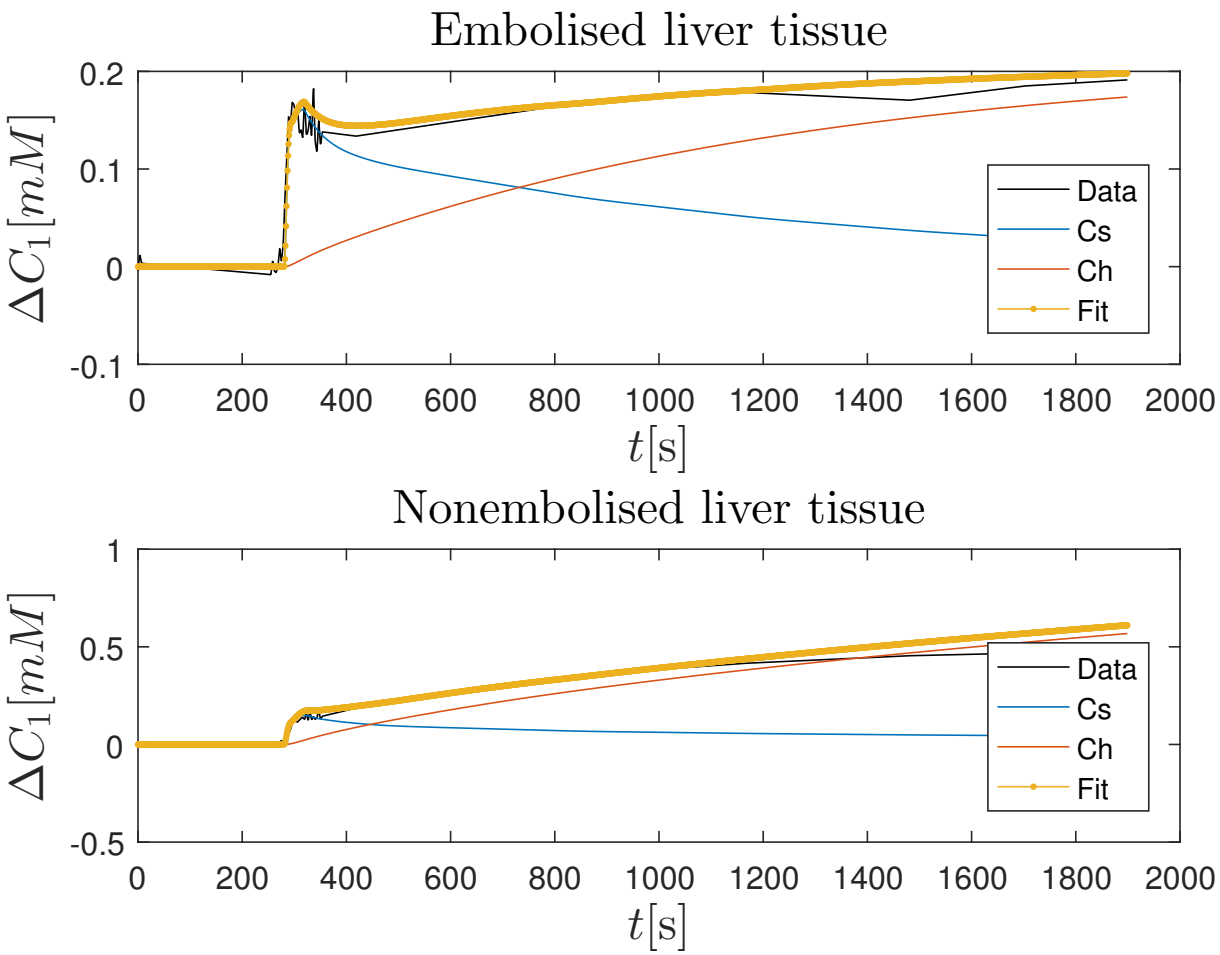

Figure 5.2: Results of fitting liver tissue signal time curves with dual-inlet two-compartment uptake model [1900 s]; on the graph it is able to notice deviation between data and fitted curve in saturation (Patient 9)

or decrease (Leonidas Georgiou 2017). Parameters which reflects physiological processes that occur at the beginning of imaging process, like perfusion and uptake rate, decreased with with acquisition duration. Differences between acquisition duration for 2CUM are shown in nonembolised healthy tissue; value of perfusion reduced on 38.2±16.4 with increased time (P=0.001). There is slightly difference between uptake rates obtained with 2CUM[600] and 2CUM[AD] in nonembolised part of the liver but p-value indicate that difference is not significant (P=0.12). By increasing duration, mean arterial flow fraction largely increased on 46.8±8.6 against the value in last case (P=0.001). This value is

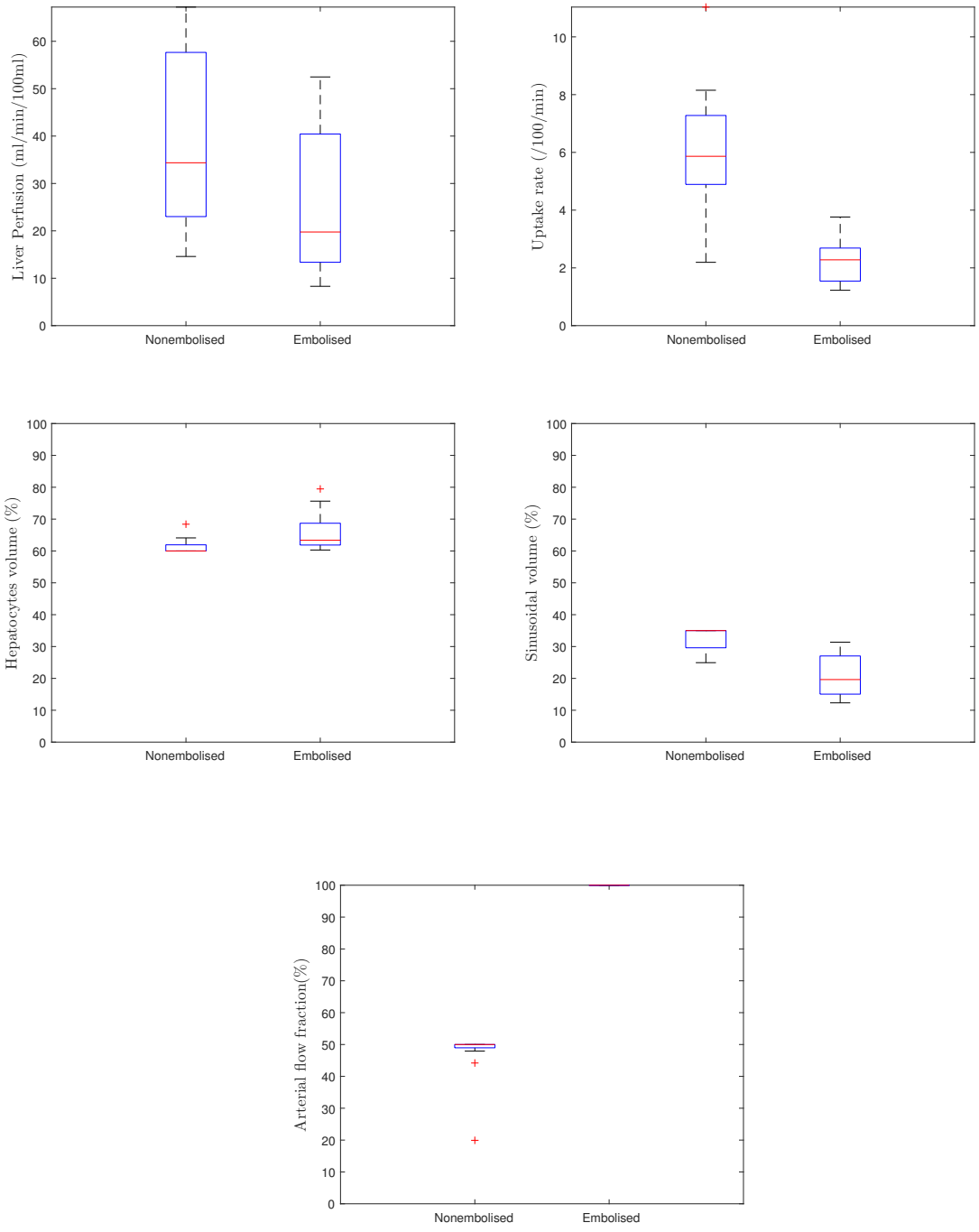

Figure 5.3: Parameters values given with dual-inlet two compartment model in acquisition duration of 1700 s

obviously incorrect. Other values for both embolised and nonembolised part of the liver, like volumes, remains the same despite the change of acquisition time (P>0.05) but if fitting space was larger, differences would probably grow. Larger acquisition time will be more important in case of extraction rate estimation. Figure 5.3 shows results for embolised and nonembolised tissue in boxplots, while Figure 5.4 shows differences in perfusion and arterial flow fraction in dependence of acquisition duration.

Table 5.5: Statistical results for 2CUM[AD]

	F[ml/min/100ml]		v_s[%]		v_h[%]	
	NEmb	Emb	NEmb	Emb	NEmb	Emb
Median	34.4	19.8	35	19.6	60	63.4
Mean	38.2	26.3	32.7	20.7	61.4	65.9
Standard deviation	19.4	15.6	3.6	6.9	2.7	6.1

	K_i[ml/min/100ml]		f_a[%]	
	NEmb	Emb	NEmb	Emb
Median	5.9	2.3	50	100
Mean	6	2.2	46.8	100
Standard deviation	2.3	0.8	8.6	0

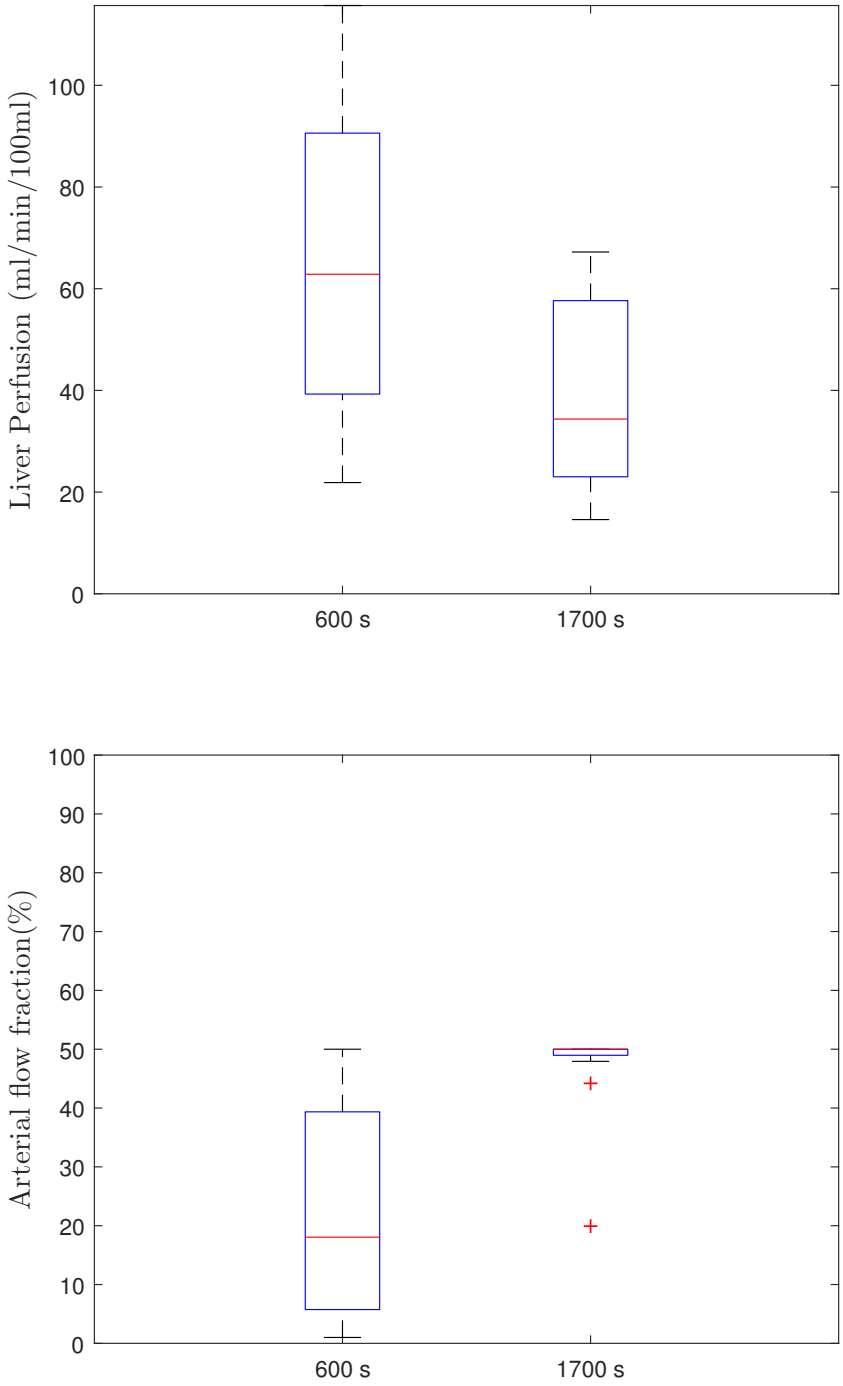

Figure 5.4: Comparison of the values of perfusion and arterial flow fraction in nonembolised tissue depending on acquisition duration

5.3 2CUMEX[AD]

Double-inlet two compartment uptake model with extraction rate describes signal time curves with six parameters. This model use whole acquisition duration, maximal and different for every patient (approximate 1700 seconds). Results for this model are shown in Table 5.6. Perfusion is 69.7±32.3 and 26.7±15.9 for nonembolised and embolised tissue. These values are significantly different (P=0.004). From all wide space fitting methods, this one gives values for sinusoidal volume closest to literature values; 28±6.9 and 20±6.3. Like in every case values are bigger in nonembolised tissue (P=0.007). Hepatocytes volume is 63.7±3.9 for nonembolised and 73.4±6.9 for embolised. Difference between volumes is also statistically significant (P=0.0003). Uptake rate and extraction rate in embolised tissue is minor compared to nonembolised tissue (P<0.0001). Values for uptake rate are 9.4±3.9 and 2.4±0.9 and for extraction rate 2.7±1.6 and 0.2±0.4. Arterial flow fraction is 20.6±19.7. Standard deviation is pretty big, like in 2CTUM[600], what means that values are widely spread. All results are represented graphically in Figure 5.5

Table 5.6: Statistical results for 2CUMEX[AD]

	F[ml/min/100ml]		v_s[%]		v_h[%]	
	NEmb	Emb	NEmb	Emb	NEmb	Emb
Median	71.6	20.5	28.8	19.5	62.8	73.7
Mean	69.7	26.7	28	20	63.7	73.4
Standard deviation	32.3	15.9	6.9	6.3	3.9	6.9

	K_i[ml/min/100ml]		K_e[ml/min/100ml]		f_a[%]	
	NEmb	Emb	NEmb	Emb	NEmb	Emb
Median	9	2.4	2.3	0.06	14.3	100
Mean	9.4	2.4	2.7	0.2	20.6	100
Standard deviation	3.9	0.9	1.6	0.4	19.7	0

Table 5.3 shows that embolised tissue is better described with 2CUM[AD] but for nonembolised tissue curves are better fitted with 2CUMEX[AD]. When comparing parameters obtained by these two models, there is no statistically significant difference between values in embolised tissue. Only significant difference is hepatocytes volume (P=0.009). Hepatocytes volume obtained with 2CUMEX[AD] and literature value ($v_h = 74\%$) considered to be not statistically significant. In other words, 2CUMEX model gave more correct value then 2CUM[AD].

When comparing parameter values obtained with 2CUM[600] and 2CUMEX[AD] there is no significant difference between them in both embolised and nonembolised tissue. Only difference is hepatocyte volume (P=0.002) witch is more correct in 2CUMEX[AD]. For most of the parameters, it is not possible to be sure about correct value, but advantage of this model is that it distinguish all values for embolised and nonembolised tissue; there is no difference in RMS value between tissues (P=0.8).

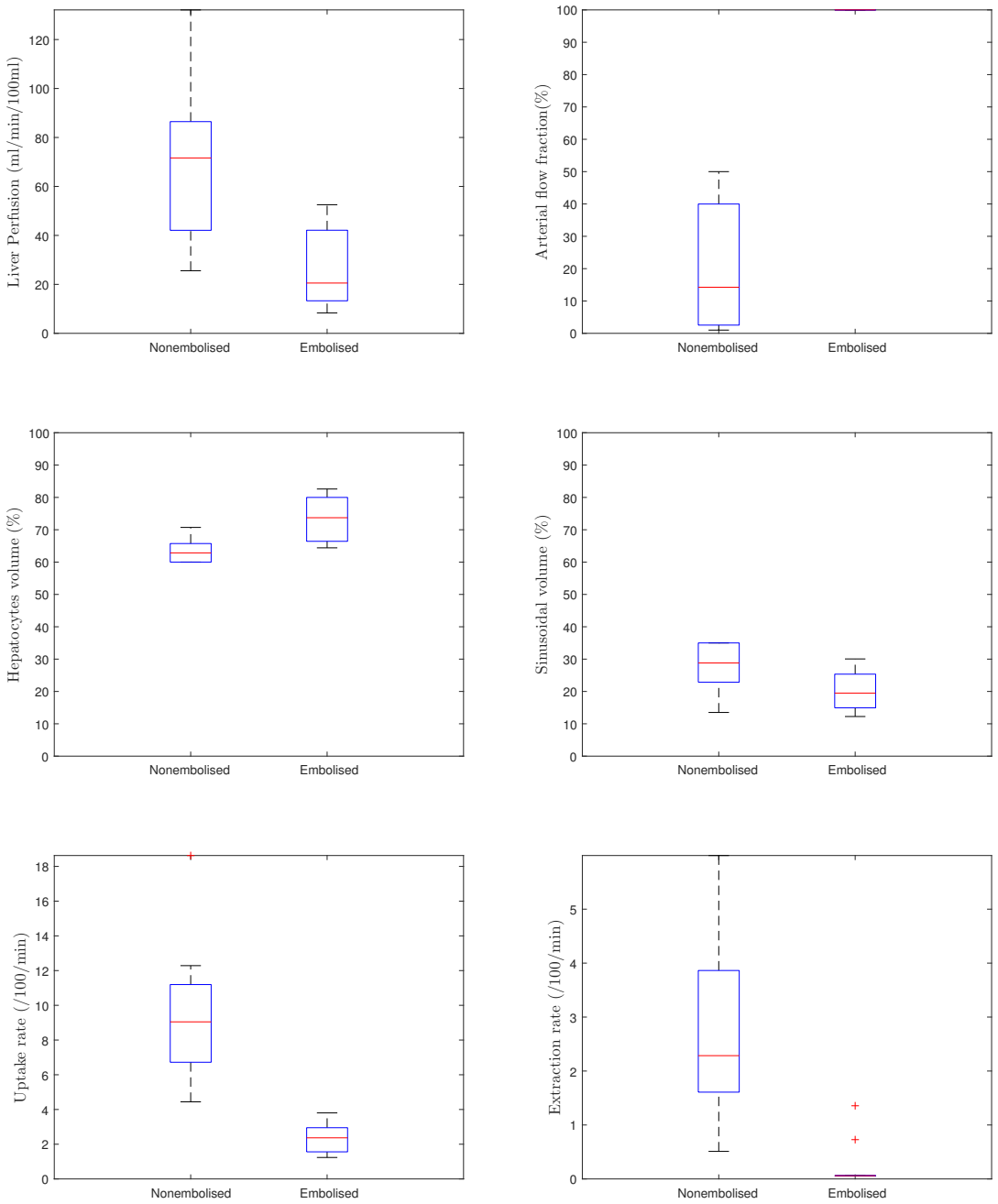

Figure 5.5: Parameters values given with dual-inlet two compartment model in acquisition duration of 600 s

5.4 Comparison of parameters between methods

Results obtained with dual-inlet two-compartment uptake model (Sourbron model) without delay as fitting parameters gave next results for the total plasma flow; F=69±30, extracellular (sinusoidal) volume; v_s=15±5,5, uptake rate K_i=3.5±2 and arterial flow fraction f_a=10±15. This model is applied on 600 seconds of acquisition duration and only difference between this and 2CUM[600] is hepatocytes volume as fitting parameter (S.P. Sourbron 2012).

In Table 5.7 it is possible to notice that results for embolised tissue is much more stable and smaller than in nonembolised tissue. Nonembolised tissue results are pretty different for each model. In case of fixed or small fitting span (LB) for volume, all models give up to four times larger values then in literature. High fitting span (HB) gives results pretty similar to literature values; there is no significant difference between perfusion values obtained with 2CUM[600](HB) or 2CUMEX[AD](HB) and literature (P=0.7, P=1), but there is difference in case of 2CUM[AD](HB) (P=0.002).

Table 5.7: Comparison of perfusion

F[ml/min/100ml]		
Method	Mean ±SD	
	NEmb	Emb
2CUM[600s], Fixed v_h, v_s	158 ±198.6	30±20.5
2CUM[600s], Fitted v_h, v_s (LB)	141±162.9	30.5±19.1
2CUM[600s], Fitted v_h, v_s (HB)	65±32.1	26.2±15.7
2CUM[AD], Fixed v_h, v_s	54.4±30.2	31.5±23.7
2CUM[AD], Fitted v_h, v_s (LB)	53.1±29.9	31.6±21.6
2CUM[AD], Fitted v_h, v_s (HB)	38.2±19.4	26.3±15.5
2CUMEX[AD], Fixed v_h, v_s	337.1±494.2	30±20.2
2CUMEX[AD], Fitted v_h, v_s (LB)	319.2±511.4	29.8±20.3
2CUMEX[AD], Fitted v_h, v_s (HB)	69.7±32.3	26.7±15.9

When it comes to volume, best result are obtained with models in case of smaller fitting space (LB), but at the same time these models are bad for others parameters (Table 5.8, Table 5.9). Methods which were using large fitting span (HB) gave real fitted parameters but there is significant difference from literature values (P>0.05). The role of this fitted parameters was to give freedom to the model. Past researches (Jian-Feng Yang 2016) showed that Tofts models are much more stable in measuring the volume, while dual-input two-compartment model is more accurate in measuring perfusion.

Table 5.8: Comparison of sinusoidal volume

$v_s[\%]$		
Method	Mean ±SD	
	NEmb	Emb
2CUM[600s], Fixed v_h, v_s	16	16
2CUM[600s], Fitted v_h, v_s (LB)	16.7±0.5	16.4±0.7
2CUM[600s], Fitted v_h, v_s (HB)	29.5±6.3	22±6.9
2CUM[AD], Fixed v_h, v_s	16	16
2CUM[AD], Fitted v_h, v_s (LB)	16.8	16.2±0.8
2CUM[AD], Fitted v_h, v_s (HB)	32.7±3.6	20.7±6.9
2CUMEX[AD], Fixed v_h, v_s	16	16
2CUMEX[AD], Fitted v_h, v_s (LB)	16.5±0.6	16.2±0.8
2CUMEX[AD], Fitted v_h, v_s (HB)	28±6.9	20±6.3

Table 5.9: Comparison of hepatocyte volume

v_h[%]		
Method	Mean ±SD	
	NEmb	Emb
2CUM[600s], Fixed v_h, v_s	74	74
2CUM[600s], Fitted v_h, v_s (LB)	73.9±2.5	74±2.1
2CUM[600s], Fitted v_h, v_s (HB)	63.1±4.6	65.3±4.4
2CUM[AD], Fixed v_h, v_s	74	74
2CUM[AD], Fitted v_h, v_s (LB)	74.2±2.4	72.3±1.6
2CUM[AD], Fitted v_h, v_s (HB)	61.4±2.7	65.9±6.1
2CUMEX[AD], Fixed v_h, v_s	74	74
2CUMEX[AD], Fitted v_h, v_s (LB)	74.6±2.2	75±2.3
2CUMEX[AD], Fitted v_h, v_s (HB)	63.7±3.9	73.4±6.9

In Table 5.10 we can see that 2CUM[AD] case give extremely high values for arterial flow fraction and they are hitting upper boundary in fitting span. All values obtained with 2CUM cases pretty differ from literature (P<0.05). Values obtained with 2CUMEX cases are not significantly different then values obtained with Sourbron model (P>0.05). Between them, 2CUMEX[AD] fixed and 2CUMEX[AD](LB) are most similar to literature values (P=0.9).

Table 5.10: Comparison of arterial flow fraction

f_a[%]		
Method	Mean ±SD	
	NEmb	Emb
2CUM[600s], Fixed v_h, v_s	24.8±23.6	100
2CUM[600s], Fitted v_h, v_s (LB)	25.2±23.6	100
2CUM[600s], Fitted v_h, v_s (HB)	22±19.4	100
2CUM[AD], Fixed v_h, v_s	48.1±4.7	100
2CUM[AD], Fitted v_h, v_s (LB)	48.4±3.8	100
2CUM[AD], Fitted v_h, v_s (HB)	46.8±8.6	100
2CUMEX[AD], Fixed v_h, v_s	9.5±16	100
2CUMEX[AD], Fitted v_h, v_s (LB)	9.7±15.3	100
2CUMEX[AD], Fitted v_h, v_s (HB)	20.6±19.7	100

5.5 K_i/K_e

Sourbron model without delay as fitting parameters obtain value of uptake rate K_i=3.5±2 (S.P. Sourbron 2012). All values differ between embolised and nonembolised tissue. There is extremely difference between all obtained values and literature. HB cases from every method gave smallest result, but in general 2CUM[AD] obtained values most similar to the literature.

Liver function can be described as ratio between uptake rate and efflux rate. This ratio could show is liver manage to preform it's tasks and how fast it can preform it. It quantifies the loss of contrast agent during its passage through the liver. Comparing to literature values (Leonidas Georgiou 2017) on healthy patients using same tracer (K_i=22±5 ml/min/100ml, K_e=1.7±0.6 ml/min/100ml $^{K_i}/_{K_e}$=12.9), mine results are giving smaller ratios; showed in Table 5.13.

The reason for that are small K_i and high K_e values is that all patients in my case suffer from primary cancer or metastases on the liver, what probably affect

on decreasing of uptake rate and increasing of extraction rate.

Table 5.11: Comparison of uptake rate

K_i[ml/min/100ml]		
Method	Mean ±SD	
	NEmb	Emb
2CUM[600s], Fixed v_h, v_s	9.4±3.5	3.2±2.1
2CUM[600s], Fitted v_h, v_s (LB)	9.4±3.4	2.9±1.6
2CUM[600s], Fitted v_h, v_s (HB)	7.9±3.4	1.9±1.2
2CUM[AD], Fixed v_h, v_s	6.4±2.1	3.2±3.2
2CUM[AD], Fitted v_h, v_s (LB)	6.4±2.1	2.4±0.8
2CUM[AD], Fitted v_h, v_s (HB)	6±2.3	2.2±0.8
2CUMEX[AD], Fixed v_h, v_s	12.1±5.2	4.9±5.3
2CUMEX[AD], Fitted v_h, v_s (LB)	11.9±5.1	3±1.3
2CUMEX[AD], Fitted v_h, v_s (HB)	9.4±3.9	2.4±0.9

Table 5.12: Comparison of extraction rate

K_e[ml/min/100ml]		
Method	Mean ±SD	
	NEmb	Emb
2CUMEX[AD], Fixed v_h, v_s	5.5±3.4	1.9±2.1
2CUMEX[AD], Fitted v_h, v_s (LB)	5.5±3.5	1.2±1.5
2CUMEX[AD], Fitted v_h, v_s (HB)	2.7±1.6	0.2±0.4

Table 5.13: Ratio of uptake rate and extraction rate

K_i/K_e		
Method	NEmb	Emb
2CUMEX[AD], Fixed v_h, v_s	2.2	2,5
2CUMEX[AD], Fitted v_h, v_s (LB)	2,2	2,5
2CUMEX[AD], Fitted v_h, v_s (HB)	3,5	12

6 Conclusion

Most of the results I have obtained in this research are in range with the values in literature. It is difficult to compare which method gives the most accurate results. While comparing the methods, some of them showed bad on t-test, but at the same time yielded results closer to the literature.

There was a lot of different settings in processing data and fitting routine which could have effect on the finishing results. One of the most important, but also demanding phase, was choosing ROI. There is no universal way for masking the area on MR images and there has to be some deviations for each patient.

Besides that, big influence on the fitting procedure is delay time. In my case delay was not fitting parameter because it was making the model very unstable. Researches has showed importance of including delay in modeling. It can cause significant difference in perfusion and arterial fraction. This research is made with dual-input single compartment model and they suggest using pre-estimation of delays with constrained free modelling (Manil Chouhan 2016). During modelling I tried to use similar technique to get results but since 2CUMEX is complex method with more parameters whole model was unstable. In some of past researches for accurately fit only arterial delay was used. Since both portal vein and artery has delay, I included them as constant.

One more thing that effect the fitting routine is time resolution which is in our case one second. When using larger time resolution, I could not obtain good fit. Original time resolution of data was around 3 seconds, but after interpolation I set time resolution on 1 second which gave me satisfying fit with small mistake.

It would be good if dynamic TWIST sequence had acquisition duration longer then 1900 seconds. If endurance of imaging was 30 to 40 minutes I could see better dependence of parameters on the time. Fitting routine with 2CUM in distinction of 1000 seconds showed significant difference between values 2 values; perfusion and arterial flow fraction. One more advantage of longer endurance would be more correct extraction rate because it would be possible to see how long does the contrast agent retained in the liver.

When there is a need for distinguishing embolised and nonembolised tissue, best model for this would be dual-inlet two-compartment uptake model with extraction rate. Results of t-test showed that there is significantly deviation between parameter values in different tissue, what was the aim of my research.

Literature

A.C.Guyton 2006

A.C.GUYTON, J.E.Hall: *Textbook of Medical Physiology*. ELSEVIER SAUNDERS, 2006

A.Haase 1986

A.HAASE, D.Matthaei W. Hänicke K.D. M. J. Frahm F. J. Frahm: FLASH Imaging. Rapid NMR Imaging Using Low Flip-Angle Pulse. In: *Journal of magnetic resonance* 67 (1986), S. 258–266

Bernard E. Van Beers 2012

BERNARD E. VAN BEERS, H.K. H. C.M. Pastor P. C.M. Pastor: Primovist, Eovist: What to expect? In: *Journal of hepatology* 57 (2012), S. 421—-429

Butzek 2014

BUTZEK, Sebastian: Evaluation einer elastischen Registrationsmethode bei mit Leberbrachytherapie bestrahlten Patienten. (2014), S. 8, 13

Catherine Westbrook 2011

CATHERINE WESTBROOK, John T. Carolyn Kauh Roth R. Carolyn Kauh Roth: *MRI in practice*. WILEY-BLACKWELL, 2011 (International series of monographs on physics)

D. Geisel 2015

D. GEISEL, B. Hamm T. D. L. Lüdemann L. L. Lüdemann: Imaging-based

liver Function Tests - past, present and future. In: *Fortschr Röntgenstr* 863–871 (2015)

David Stark 1999

DAVID STARK, William B.: *Magnetic Resonance Imaging*. Mosby, 1999

Forsgren 2017

FORSGREN, Mikael F.: *The Non-Invasive Liver Biopsy, Determining Hepatic Function in Diffuse and Focal Liver Disease*. Linköping University, 2017 (International series of monographs on physics). – 71 S.

Gerhard Laub 2006

GERHARD LAUB, Randall K.: Syngo TWIST for Dynamic Time-Resolved MR Angiography. In: *Clinical Cardiovascular* 3 (2006), S. 92–95

Jens Frahm 1986

JENS FRAHM, Dieter M. Axel Haase H. Axel Haase: Rapid NMR Imaging of Dynamic Processes Using the FLASH Technique. In: *Magnetic resonance in medicine* 3 (1986), S. 321–327

Jesper F. Kallehauge 2017

JESPER F. KALLEHAUGE, Benjamin Irving Kari Tanderup Julia A. Schnabel Michael A. C. Steven Sourbron S. Steven Sourbron: Comparison of Linear and Nonlinear Implementation of the Compartmental Tissue Uptake Model for Dynamic Contrast-Enhanced MRI. In: *Magnetic Resonance in Medicine* 77 (2017), S. 414–2423

Jian-Feng Yang 2016

JIAN-FENG YANG, Yu Zhang Li Zhao Li-Ming Yang Min-Ming Zhang Bo-Yin Wang Ting Wang Bao-Chun L. Zhen-Hua Zhao Z. Zhen-Hua Zhao: Dual-input two-compartment pharmacokinetic model of dynamic contrast-

enhanced magnetic resonance imaging in hepatocellular carcinoma. In: *World Joural of Gastroenterology* 22 (2016), S. 3652–3662

J.Sear 1992

J.SEAR: Anatomy and physiology of the liver. In: *Baillidre's ClinicaI Anaesthesiology* 6 (1992), S. 697–727

Ka-Loh Li 2000

KA-LOH LI, John Waterton Alan J. Xiao Ping Zhu Z. Xiao Ping Zhu: Improved 3D Quantitative Mapping of Blood Volume and Endothelial Permeability in Brain Tumors. In: *Journal of magnetic resonance imaging* 12 (2000), S. 347–357

L. Lüdemann 2000

L. LÜDEMANN, C. Z. B. Hamm H. B. Hamm: Pharmacokinetic analysis of glioma compartments with dynamic Gd-DTPA-enhanced magnetic resonance imaging. In: *Magnetic resonance imagining* 18 (2000), S. 1201–1214

Leonidas Georgiou 2017

LEONIDAS GEORGIOU, Glynis Nicholls Neil Woodhouse François-Xavier Blé-Penny L. Hubbard Cristinacce Josephine N. Jeffrey Penny P. Jeffrey Penny: Quantitative Assessment of Liver Function Using Gadoxetate-Enhanced Magnetic Resonance Imaging: Monitoring Transporter-Mediated Processes in Healthy Volunteers. In: *Investigative Radiology* 52 (2017), S. 111–119

Madsen 1992

MADSEN, Mark: A simplified formulation of the gamma variate function. In: *Physics in medicine biology* 37 (1992), S. 1597–1600

Manil Chouhan 2016

MANIL CHOUHAN, David Atkinson Shonit Punwani Rajeshwar Mookerjee

Mark Lythgoe4 Stuart T. Alan Bainbridge B. Alan Bainbridge: Estimation of contrast agent bolus arrival delays for improved reproducibility of liver DCE MRI. In: *Physics in Medicine Biology* 61 (2016), S. 6905–6918

Martin Rohrer 2005

MARTIN ROHRER, Jan Mintorovitch Martin Requardt Hanns-Joachim W. Hans Bauer B. Hans Bauer: Comparison of Magnetic Properties of MRI Contrast Media Solutions at Different Magnetic Field Strengths. In: *Invest Radiol* 40 (2005), S. 715–724

The University of Meine

MEINE, Department of C. o.: *Magnetic Moments for Spin*. `http://chemistry.umeche.maine.edu/CHY431/NMR/NMR-3.html`

Michale Markl 2012

MICHALE MARKL, Jochen L.: Gradient Echo Imaging. In: *Journal of magnetic resonance imagining* 35 (2012), S. 1274–1289

OpenStax College 2013

OPENSTAX COLLEGE, Rice U.: *Anatomy Physiology*. 2013

P. Kletting 2009

P. KLETTING, G. G.: Model selection for time-activity curves: the corrected Akaike information criterion and the F-test. In: *Medizinische Physik* 19 (2009), S. 200–206

Poldrack 2007

POLDRACK, Russell A.: Region of interest analysis for fMRI. In: *SCAN* 2 (2007), S. 67–70

Pubchem

PUBCHEM: *Primosvist*. `https://pubchem.ncbi.nlm.nih.gov/compound/91754427#section=Top`

Renz 2003

RENZ, Harald: *Integrative Klinische Chemie und Laboratoriumsmedizin: Pathophysiologie, Pathobiochemie, Hämatologie*. Walter de Gruyter, 2003

Romaric Loffroy 2015

ROMARIC LOFFROY, Olivier Chevallier Louis Estivalet Pierre-Yves Genson Pierre Pottecher Sophie Gehin Denis Krausé-Jean-Pierre C. Sylvain Favelier F. Sylvain Favelier: Preoperative portal vein embolization in liver cancer: indications, techniques and outcomes. In: *Quantitative Imaging in Medicine and Surgery* 5 (2015), S. 730–739

S.P. Sourbron 2012

S.P. SOURBRON, M.F. Reiser C.J. Z. W.H. Sommer S. W.H. Sommer: Combined quantification of liver perfusion and function with dynamic gadoxetic acid-enhanced MR imaging. In: *Radiology* 263 (2012), S. 874–883

S.P.Sourbron 2011a

S.P.SOURBRON, D.L.Buckley: Tracer kinetic modelling in MRI: estimating perfusion and capillary permeability. In: *Physics in medicine biology* 57 (2011), S. R1–R33

S.P.Sourbron 2011b

S.P.SOURBRON, M.F. Reiser C.J. Z. W.H. Sommer S. W.H. Sommer: Tracer kinetic modelling in MRI: estimating perfusion and capillary permeability. In: *Physics in medicine biology* 57 (2011), S. R1–R33

Thomas Benner 1997

THOMAS BENNER, Guner Erb Michael Forsting Klaus S. Sabine Heiland H. Sabine Heiland: Accuracy of gamma-variate fits to concentration-time curves from dynamic susceptibility contrast enhanced MRI: Influence of the

time resolution, maximal signal drop and signal-to-nosie. In: *Magnetic resonance imagining* 15 (1997), S. 307–317

Tofts u. a. 1999

TOFTS, P. S. ; BRIX, G. ; BUCKLEY, D. L. ; EVELHOCH, J. L. ; HENDERSON, E. ; KNOPP, M. V. ; LARSSON, H. B. ; LEE, T. Y. ; MAYR, N. A. ; PARKER, G. J. ; PORT, R. E. ; TAYLOR, J. ; WEISSKOFF, R. M.: Estimating kinetic parameters from dynamic contrast-enhanced T(1)-weighted MRI of a diffusable tracer: standardized quantities and symbols. In: *Journal of magnetic resonance imaging* 10 (1999), Sep, Nr. 3, 223–232. `http://www.ncbi.nlm.nih.gov/pubmed/10508281`. – ISSN 1053–1807

Yee Liang Thiana 2013

YEE LIANG THIANA, Dow-Mu K. Angela M. Riddellb R. Angela M. Riddellb: Liver-specific agents for contrast-enhanced MRI: role in oncological imaging. In: *Cancer Imaging* 13 (2013), S. 567–579

Ylva Lilja 2016

YLVA LILJA, Maria Ljungberg Daniel Nilsson Göran S. Oscar Gustafsson G. Oscar Gustafsson: Impact of region-of-interest method on quantitative analysis of DTI data in the optic tracts. In: *BMC Medical Imaging* 16:42 (2016)

Zahif 2014

ZAHIF, Abdelilah: Untersuchung der Schlüssellochtechnik bei k-Raumabtastung von dynamischen kontrastmittelbasierten Magnetresonanztomographien. (2014), S. 12, 34

Zylka 2013

ZYLKA, Patrick: Pharmakokinetische Modellierung eines leberspezischen Kontrastmittels. (2013), S. 29–31

Appendices

A Fitting codes

A.1 AIF signal time curve fitting routine

```
! deltat: time step
! deltazeit: arrival of the first bolus
! deltazeit2: arrival of the second bolus
! ampl: amplitude of the first bolus
! ampl2: amplitude of the second bolus
! SecBolWdth: manually input parameter witch enables manipulation of
   the fit
! x(1): first bolus rise
! x(2): first bolus fall
! x(3): time of maximum of the first bolus
! x(4): first bolus intensity
! x(5): saturation intensity
! x(6): saturation fall
! x(7): saturation width - manually input parameter
! x(8): time shift of the exponential decay of saturation -manually
   input parameter
! x(9): time of maximum of the second bolus
! x(10): second bolus intensity
! x(11): second bolus rise
! x(12): second bolus fall

do j=0,int(deltat(k))
    deltazeit=zeit+dble(j)-x(3)+x(1)/x(2)
```

```
    deltazeit2=15+zeit+dble(j)-x(9)+x(11)/x(12)

! First bolus
    if ((deltazeit.gt.0).and. (deltazeit.lt. 15)) then
        if (j.eq.int(deltat(k))) then
        ergeb=ergeb+(deltat(k)-int(deltat(k)))*ampl
        *deltazeit**x(1)*dexp(-deltazeit*x(2))/deltat(k)
        endif
        else
        ergeb=ergeb+ampl*deltazeit**x(1)
        *dexp(-deltazeit*x(2))/deltat(k)
        endif
! Second bolus
    else if ((deltazeit.ge. 15).and. (deltazeit2 .lt. SecBolWdth))
       then
        if (j.eq.int(deltat(k))) then
        ergeb=ergeb+(deltat(k)-int(deltat(k)))*ampl2*
        deltazeit**x(11)*dexp(-deltazeit*x(12))/deltat(k)
        endif
        else
        ergeb=ergeb+ampl2*deltazeit**x(11)
        *dexp(-deltazeit*x(12))/deltat(k)
        endif
! Saturation
    else if (deltazeit2.ge. SecBolWdth) then
        ergeb=ergeb+(deltat(k)-int(deltat(k)))+x(5)
        *dexp(((15+SecBolWdth)-deltazeit)/x(6))
        endif
enddo
```

A.2 PVIF signal time curve fitting routine

```
! deltat: time step
! deltazeit: arrival of the first bolus
! ampl: amplitude of the first bolus
! SecBolWdth: manually input parameter witch enables manipulation of
   the fit
! x(1): first bolus rise
! x(2): first bolus fall
! x(3): time of maximum of the first bolus
! x(4): first bolus intensity
! x(5): saturation intensity
! x(6): saturation fall
! x(7): saturation width - manually input parameter
! x(8): time shift of the exponential decay of saturation - manually
   input parameter

do j=0,int(deltat(k))
    deltazeit=zeit+dble(j)-x(3)+x(1)/x(2)

! First bolus
    if ((deltazeit.gt.0) .and. (deltazeit .lt. SecBolWdth)) then
        if (j.eq.int(deltat(k))) then
        ergeb=ergeb+(deltat(k)-int(deltat(k)))*ampl
        *deltazeit**x(1)*dexp(-deltazeit*x(2))/deltat(k)
        endif
        else
        ergeb=ergeb+ampl*deltazeit**x(1)
        *dexp(-deltazeit*x(2))/deltat(k)
        endif
! Saturation
    else if (deltazeit.ge. SecBolWdth) then
        ergeb=ergeb+x(5)*dexp((SecBolWdth-deltazeit)/x(6))/deltat(k)
        endif
enddo
```

A.3 Fitting routine (2CUM)

```
% x0 initual values
% lb initual values for lower boundrey
% ub initual values for upper boundrey
% Finput
% vs
% Ki
% vh
% fa
% A, b are condition matrix for sum of hepatocytes and sinusoidal
   volume
% tolx: convergevce tolerance on solution vector, if the solver
   attempts to take a step that is smaller than tolx, the iterations
   end
% tolf: convergence tolarance on function value
% createOptimProblem: creates an empty optimization problem structure
% fmincon: the type of solver and
% objective: function which accepts vector and returns a scalar
% MultiStart: solver attempts to find multiple local solutions
% UseParallel: distribute local solver calls to multiple processors

x0 = [ Finput    vs     Ki      vh    fa    ];
lb = [ Finput_lb vs_lb  Ki_lb   vh_lb fa_lb ];
ub = [ Finput_ub vs_ub  Ki_ub   vh_ub fa_ub ];

A = [ 0 1 0 1 0 0 ];
b = [ 0.95 ];


tolx=1e-3;tolf=1e-6;
opts = optimset('Algorithm','sqp','TolX',tolx,'TolFun',tolf);
problem = createOptimProblem('fmincon','objective',
@(x)SourbronM_Ke_ODE_func(x,time_data,signal_data,name,emb),
'x0',x0,'Aineq',A,'bineq',b,'lb',lb,'ub',ub,'options',opts);
ms = MultiStart('UseParallel','always');
[x RMS] = run(ms,problem,4000);
```

```
for n = 1:length(t)-1
    Cs(n+1) = (Finput/vs)*((1-fa)*pvif_corr(n)
       +fa*aif_corr(n))*dt-Cs(n)*((Ki+Finput/vs))*dt+Cs(n);
    Ch(n+1) = (Ki/vh)*Cs(n)*dt+Ch(n);
end

Cs = vs*Cs;
Ch = vh*Ch;
Ct = Cs+Ch;
```

A.4 Fitting routine (2CUMEX)

```
% x0 initual values
% lb initual values for lower boundrey
% ub initual values for upper boundrey
% Finput
% vs
% Ki
% vh
% fa
% Ke
% A, b are condition matrix for sum of hepatocytes and sinusoidal
   volume
% tolx: convergevce tolerance on solution vector, if the solver
   attempts to take a step that is smaller than tolx, the iterations
   end
% tolf: convergence tolarance on function value
% createOptimProblem: creates an empty optimization problem structure
% fmincon: the type of solver and
% objective: function which accepts vector and returns a scalar
% MultiStart: solver attempts to find multiple local solutions
% UseParallel: distribute local solver calls to multiple processors

x0 = [ Finput    vs     Ki      vh    fa    Ke ];
lb = [ Finput_lb vs_lb  Ki_lb   vh_lb fa_lb Ke_lb ];
ub = [ Finput_ub vs_ub  Ki_ub   vh_ub fa_ub Ke_ub ];

A = [ 0 1 0 1 0 0 ];
b = [ 0.95 ];


tolx=1e-3;tolf=1e-6;
opts = optimset('Algorithm','sqp','TolX',tolx,'TolFun',tolf);
problem = createOptimProblem('fmincon','objective',
@(x)SourbronM_Ke_ODE_func(x,time_data,signal_data,name,emb),
'x0',x0,'Aineq',A,'bineq',b,'lb',lb,'ub',ub,'options',opts);
```

```
ms = MultiStart('UseParallel','always');
[x RMS] = run(ms,problem,4000);


for n = 1:length(t)-1
    Cs(n+1) = (Finput/vs)*((1-fa)*pvif_corr(n)+
        fa*aif_corr(n))*dt-Cs(n)*((Ki+Finput)/vs)*dt+Cs(n);
    Ch(n+1) = (Ki/vh)*Cs(n)*dt-(Ke/vh)*Ch(n)*dt+Ch(n);
end

Cs = vs*Cs;
Ch = vh*Ch;
Ct = Cs+Ch;
```

B Resulting values of all examined methods

Table B.1: 2CUM[600] Fixed volume

	F[ml/min/100ml]		v_s[%]		v_h[%]	
	NEmb	Emb	NEmb	Emb	NEmb	Emb
Median	81.6	27	16	16	74	74
Quantile 25	47.8	11.1	16	16	74	74
Quantile 75	138.9	43	16	16	74	74
Mean	158.6	30	16	16	74	74
Standard deviation	198.6	20.5	0	0	0	0

	K_i[ml/min/100ml]		K_e[ml/min/100ml]		f_a[%]	
	NEmb	Emb	NEmb	Emb	NEmb	Emb
Median	10.4	3.5	0	0	21.4	100
Quantile 25	6	1.4	0	0	1	100
Quantile 75	11.1	4.7	0	0	50	100
Mean	9.4	3.2	0	0	24.8	100
Standard deviation	3.5	2.1	0	0	23.6	0

Table B.2: 2CUM[600] Fitted volume LB

	F[ml/min/100ml]		v_s[%]		v_h[%]	
	NEmb	Emb	NEmb	Emb	NEmb	Emb
Median	80.3	25.1	16.8	16.8	73.3	73.6
Quantile 25	45.4	17.4	16.8	15.8	72	72.4
Quantile 75	129.8	41.9	16.8	16.8	76.4	75.7
Mean	141	30.5	16.7	16.4	73.9	74
Standard deviation	162.9	19.1	0.5	0.7	2.5	2.1

	K_i[ml/min/100ml]		K_e[ml/min/100ml]		f_a[%]	
	NEmb	Emb	NEmb	Emb	NEmb	Emb
Median	10.3	3	0	0	23.9	100
Quantile 25	6.1	1.8	0	0	1	100
Quantile 75	11	3.7	0	0	50	100
Mean	9.4	2.9	0	0	25.2	100
Standard deviation	3.4	1.6	0	0	23.6	0

Table B.3: 2CUM[600] Fitted volume HB

	F[ml/min/100ml]		v_s[%]		v_h[%]	
	NEmb	Emb	NEmb	Emb	NEmb	Emb
Median	62.8	20.6	31	20.7	61.9	65.3
Quantile 25	39.3	13.1	27	16.8	60	61
Quantile 75	90.6	40.9	35	26.2	64.3	68.5
Mean	65.5	26.2	29.5	22	63.1	65.3
Standard deviation	32.1	15.7	6.3	6.9	4.6	4.4

	K_i[ml/min/100ml]		K_e[ml/min/100ml]		f_a[%]	
	NEmb	Emb	NEmb	Emb	NEmb	Emb
Median	7.6	2.2	0	0	18	100
Quantile 25	6	1	0	0	5.7	100
Quantile 75	9.3	2.7	0	0	39.4	100
Mean	7.9	1.9	0	0	22	100
Standard deviation	3.4	1.2	0	0	19.4	0

Table B.4: 2CUM[AD] Fixed volume

	F[ml/min/100ml]		v_s[%]		v_h[%]	
	NEmb	Emb	NEmb	Emb	NEmb	Emb
Median	49	26.1	16	16	74	74
Quantile 25	27.3	17.1	16	16	74	74
Quantile 75	85	43.1	16	16	74	74
Mean	54.4	31.5	16	16	74	74
Standard deviation	30.2	23.7	0	0	0	0

	K_i[ml/min/100ml]		K_e[ml/min/100ml]		f_a[%]	
	NEmb	Emb	NEmb	Emb	NEmb	Emb
Median	6.1	2.6	0	0	50	100
Quantile 25	5.2	2	0	0	50	100
Quantile 75	7.2	3.2	0	0	50	100
Mean	6.4	3.2	0	0	48.1	100
Standard deviation	2.1	3.2	0	0	4.7	0

Table B.5: 2CUM[AD] Fitted volume LB

	F[ml/min/100ml]		v_s[%]		v_h[%]	
	NEmb	Emb	NEmb	Emb	NEmb	Emb
Median	46	26.4	16.8	16.8	74.1	72
Quantile 25	25.8	14.7	16.8	15.2	71.9	70.9
Quantile 75	83.7	41.7	16.8	16.8	76.5	74
Mean	53.1	31.6	16.8	16.2	74.2	72.3
Standard deviation	29.9	21.6	0	0.8	2.4	1.6

	K_i[ml/min/100ml]		K_e[ml/min/100ml]		f_a[%]	
	NEmb	Emb	NEmb	Emb	NEmb	Emb
Median	6.2	2.5	0	0	50	100
Quantile 25	5.2	1.7	0	0	50	100
Quantile 75	7.2	2.9	0	0	50	100
Mean	6.4	2.4	0	0	48.4	100
Standard deviation	2.1	0.8	0	0	3.8	0

Table B.6: 2CUM[AD] Fitted volume HB

	F[ml/min/100ml]		v_s[%]		v_h[%]	
	NEmb	Emb	NEmb	Emb	NEmb	Emb
Median	34.4	19.8	35	19.6	60	63.4
Quantile 25	23	13.4	29.6	15.1	60	61.9
Quantile 75	57.7	40.4	35	27	61.9	68.7
Mean	38.2	26.3	32.7	20.7	61.4	65.9
Standard deviation	19.4	15.6	3.6	6.9	2.7	6.1

	K_i[ml/min/100ml]		K_e[ml/min/100ml]		f_a[%]	
	NEmb	Emb	NEmb	Emb	NEmb	Emb
Median	5.9	2.3	0	0	50	100
Quantile 25	4.9	1.5	0	0	49	100
Quantile 75	7.3	2.7	0	0	50	100
Mean	6	2.2	0	0	46.8	100
Standard deviation	2.3	0.8	0	0	8.6	0

Table B.7: 2CUMEX[AD] Fixed volume

	F[ml/min/100ml]		v_s[%]		v_h[%]	
	NEmb	Emb	NEmb	Emb	NEmb	Emb
Median	148.2	28	16	16	74	74
Quantile 25	59.3	15.9	16	16	74	74
Quantile 75	346.4	41	16	16	74	74
Mean	337.2	30	16	16	74	74
Standard deviation	494.2	20.2	0	0	0	0

	K_i[ml/min/100ml]		K_e[ml/min/100ml]		f_a[%]	
	NEmb	Emb	NEmb	Emb	NEmb	Emb
Median	12.1	3.7	5	0.9	1	100
Quantile 25	7.3	2.2	2.6	0.1	1	100
Quantile 75	15.3	5.2	8.2	3.8	9.6	100
Mean	12.1	4.9	5.5	1.9	9.5	100
Standard deviation	5.2	5.3	3.4	2.1	16	0

Table B.8: 2CUMEX[AD] Fitted volume LB

	F[ml/min/100ml]		v_s[%]		v_h[%]	
	NEmb	Emb	NEmb	Emb	NEmb	Emb
Median	128.6	23	16.8	16.8	74.7	75.5
Quantile 25	60.8	15.4	16.8	15.3	73.2	72.7
Quantile 75	313.7	41.7	16.8	16.8	76.3	77.2
Mean	319.2	29.8	16.5	16.2	74.6	75
Standard deviation	511.4	20.3	0.6	0.8	2.2	2.3

	K_i[ml/min/100ml]		K_e[ml/min/100ml]		f_a[%]	
	NEmb	Emb	NEmb	Emb	NEmb	Emb
Median	12	2.9	4.8	0.3	1.6	100
Quantile 25	7.1	2.1	2.4	0.1	1	100
Quantile 75	15.2	3.8	8.2	2.6	11	100
Mean	11.9	3	5.5	1.2	9.7	100
Standard deviation	5.1	1.3	3.5	1.5	15.3	0

Table B.9: 2CUMEX[AD] Fitted volume HB

	F[ml/min/100ml]		v_s[%]		v_h[%]	
	NEmb	Emb	NEmb	Emb	NEmb	Emb
Median	71.6	20.5	28.8	19.5	62.8	73.7
Quantile 25	42.1	13.3	22.9	14.9	60	66.4
Quantile 75	86.5	42.1	35	25.3	65.7	80
Mean	69.7	26.7	28	20	63.7	73.4
Standard deviation	32.3	15.9	6.9	6.3	3.9	6.9

	K_i[ml/min/100ml]		K_e[ml/min/100ml]		f_a[%]	
	NEmb	Emb	NEmb	Emb	NEmb	Emb
Median	9	2.4	2.3	0.1	14.3	100
Quantile 25	6.7	1.6	1.6	0.1	2.5	100
Quantile 75	11.2	3	3.9	0.1	40	100
Mean	9.4	2.4	2.7	0.2	20.6	100
Standard deviation	3.9	0.9	1.6	0.4	19.7	0